Deciphering the morphology of turbiditic lobe bodies according to hierarchy and system size

Louison Mercier [a], Jean-Louis Grimaud [a], Fabien Ors [a]

a : PSL University, MINES Paris, Centre de Géosciences, 35 rue St Honoré, 77305 Fontainebleau Cedex, France

Louison Mercier, louison.mercier@minesparis.psl.eu

Jean-Louis Grimaud, jean-louis.grimaud@minesparis.psl.eu

Fabien Ors, fabien.ors@minesparis.psl.eu

Abstract

Turbiditic lobe bodies (LBs) are the ultimate deposits of source-to-sink systems. Their geometry and architecture vary with depositional environment (marine vs. lacustrine), hierarchy (lobe elements, lobes, lobe complexes), system size (large vs. small) and topographic confinement. Constraining these variations is useful for characterizing the dispersion of sediments, carbon, nutrients, and pollutants into lacustrine and deepwater environments. Although LBs are known to be dominantly ellipsoidal, robust statistics of scaling relationships describing their morphology are still lacking. Here, we compile data (n = 365) from seabed surface, subsurface, and outcrops of modern and ancient systems to investigate the morphometric scaling of LBs. We show that the shape of LBs is firstly controlled by the hierarchy of LBs and secondly by the system size. The LBs from large systems are one order of magnitude more voluminous than those from small systems. We demonstrate for the first time that each hierarchical level has its own elongation (i.e., length-to-width) ratio, but also its own 3D morphometric scaling where its length correlates with its width-to-thickness ratio. This is consistent with the construction of the highest hierarchy LBs dominated by the lateral stacking of lower hierarchy LBs, promoting sediment spreading in the abyssal plains and lacustrine bottoms, while aggradation is secondary.

Keywords: Turbidites, distal lobes, deep-sea systems, morphologic scaling, sink.

1. Introduction

Subaqueous fans are distal deposits composed of different scales of distributary channels (Pettinga et al., 2018; Pickering et al., 2015; Pickering and Clark, 1996) and lobe bodies (LBs) (Fig. 1) (Deptuck et al., 2008; Pettinga et al., 2018; Prélat et al., 2010, 2009; Saller et al., 2008; Sweet et al., 2019), respectively formed by channelized and unconfined gravity flows connected through a transition zone (Mutti and Normark, 1987; Wynn et al., 2002). Historically, LBs have been investigated by the oil and gas industry for hydrocarbon exploration and, more recently, for CO_2 storage because they constitute good-quality reservoirs, often in the form of stratigraphic or combined traps (Allan et al., 2006; Amy, 2019). Recent studies showed that turbiditic currents are efficient for the long-run transport (Hage et al., 2024) and burial (Talling et al., 2024) of terrestrial organic carbon. Within turbidite systems, organic matter is mainly deposited within fine-grained sand, showing a mean weighted terrestrial organic carbon with facies of 0.8 to 1 % in channel margins and lobe fringe that can reach 1.6 to 3.2 % in lobes (Hage et al., 2022; Spychala et al., 2025). Consequently, turbidite systems can store more than 60 % of the global terrestrial organic content exported to the marine environments, depending on the sea level (Talling et al., 2024). Therefore, LBs constitute a significant sink in the carbon cycle. Finally, gravity flows are also effective at transporting anthropogenic pollutants, such as microplastics, in deepwater environments (Bell et al., 2021; Chen et al., 2025; Kane and Clare, 2019), and LBs are consequently also a sink for plastic microfibers and fragments (Pohl et al., 2020b).

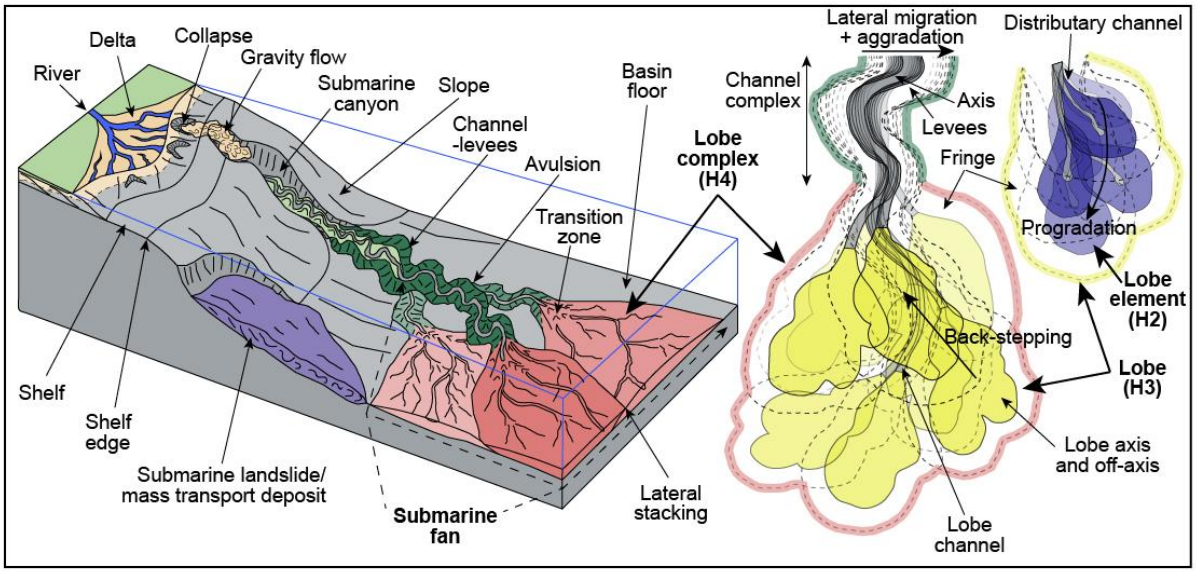

Figure 1. Diagram block of a schematic continental margin showing a sedimentary system from the delta to the distal submarine fan (modified after Talling et al. 2024), and the close-up views on a lobe complex and lobe architectures (inspired by Prélat et al., 2010; Pettinga et al., 2018). Hierarchical levels of distal lobe bodies are lobe element (H2), lobe (H3), and lobe complex (H4).

Previous studies proposed scaling relationships regarding: (i) LBs dimensions (width, length, thickness, area, and/or volumes) (Pettinga et al., 2018; Prélat et al., 2010, 2009), or (ii) feeding channels size vs LBs dimensions (Pettinga et al., 2018). Such scaling relationships provide useful insights into the intrinsic properties and processes operating in the distal part of source-to-sink systems (Sømme et al., 2009). At their depositional time-scale (i.e., 10^2-10^4 yrs) (Deptuck et al., 2008; Droz et al., 2020; Jegou et al., 2008; Jobe et al., 2017; Picot et al., 2016; Sweet et al., 2019), it was suggested that the dimensions of LBs do not correlate with those of their terrestrial feeding catchments (Pettinga et al., 2018), due (i) to avulsions (Fig. 1) that segment the size of LBs (Straub and Pyles, 2012) and (ii) to the transfer of particles that is incomplete in distal environments (Romans et al., 2016). Works that focused on the scaling of LBs mainly considered their hierarchy (i.e., lobe elements, lobes, and lobe complexes) (Fig. 1) and topographic confinement (confined vs. unconfined). It was suggested that the degrees of LBs' confinement increase with the ratio of their thickness to depositional area (Pettinga et al., 2018; Prélat et al., 2010). Nevertheless, the gravity-flow properties (i.e., volume, hydraulic regime, density, concentration, and grainsize of transported particles) were considered as the primary control on the shape of LBs (Baas et al., 2004; Talling et al., 2012; Wahab et al., 2022), with topographic confinement being a secondary factor (Al Ja'Aidi et al., 2004).

The properties of gravity flows partly depend on the system type (i.e., mud-rich vs. mud-sand-rich vs. sand-rich). Larger systems are usually thought to be less sandy and more mud-prone (Reading and Richards, 1994). Inferring system type can be done using the net-to-gross ratio (NTG: the volume of sand over the whole volume) measured on boreholes or from seismic data. In detail, small systems were considered as sand-rich (NTG > 70%), medium systems as mud/sand-rich (30 < NTG < 70%), and large systems as mud-rich (NTG < 30%) (Reading and Richards, 1994). In detail, sand vs. mud distribution may be heterogeneous within the LBs of large systems, potentially inducing a bias depending on where the NTG is measured. For instance, in the Amazon and Nile systems, the lobe axis is very sandy (NTG ≥ 70%) on a restricted width of ≈ 5-10 km (Migeon et al., 2010; Piper and Normark, 2001). Therefore, in this study and in contrast to previous works that investigated the morphometric scaling of LBs, the size of deepwater systems (i.e., small, medium, or large) is preferred over sand-richness for system comparison.

In this study, a large dataset from Permian to modern fan systems (Fig. 2, SM, database) is collected to demonstrate the influence of (i) hierarchical order, (ii) system size, and (iii) depositional environment (marine vs lacustrine) on the morphometrics of LBs. When possible, scaling relationships are defined. Then, these morphological properties are used to evaluate the processes that operate at different hierarchical scales and the differences between small and large systems.

2. Data and methods

To compare the morphology of LBs according to hierarchical levels (H2: lobe elements, H3: lobes, H4: lobe complexes) and system sizes, we complemented two existing datasets (i.e., Pettinga et al., 2018; Prélat et al., 2010) with data from the literature to obtain morphological data for LBs (n = 365) from 60 submarine-fan systems and 4 lacustrine systems (Fig. 2, SM, database). Measurements of L (length), W (width), and H (thickness) mainly come from sonar and seismic-reflection surveys (Fig. 3) and less frequently from outcrops. Area (A) is either measured or calculated, while volume (V) is systematically calculated. Below, we detail: 1) the definition and the classifications of the system types, and 2) the measurements and calculations of LBs dimensions.

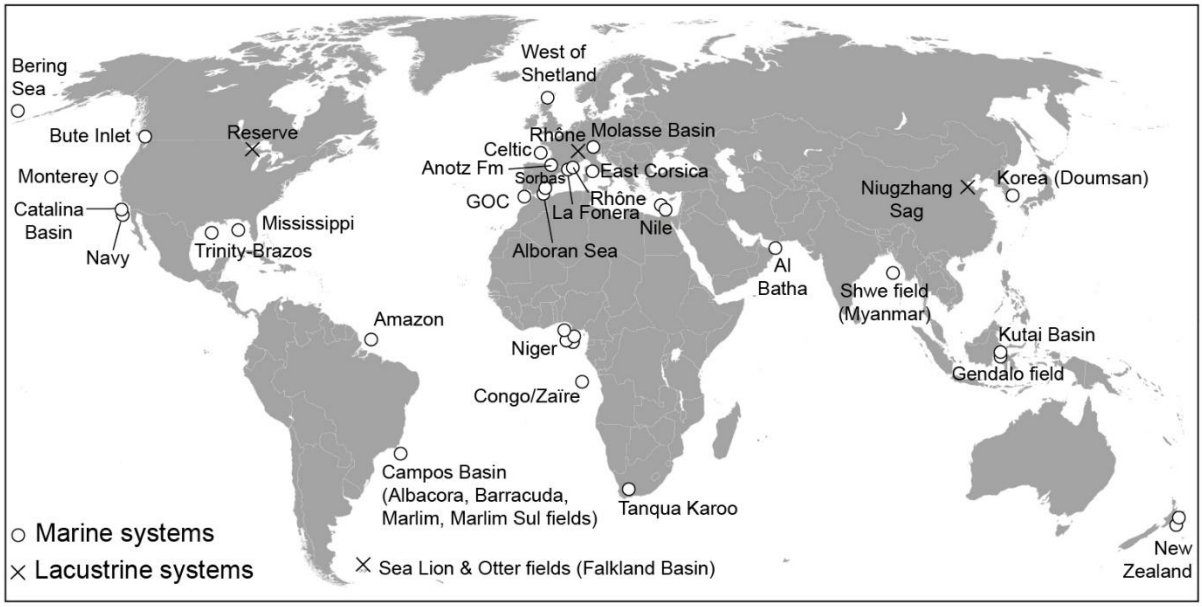

Figure 2. Geographic location of the 60 submarine and 4 lacustrine fans included in this study. The map is provided from https://www.freeimages.com/download/free-vector-world-map-5384230.

2.1. Studied systems

Systems of the dataset are from various geographic locations (Fig. 2), tectonic settings (i.e., passive, active, transform margin or aborted rift), source-to-sink configurations (i.e., basin floor vs. intraslope), and environments (i.e., marine vs. lacustrine) (SM). Note also that confined systems in intraslope settings exhibit two configurations: ponded or not ponded (SM; database). As introduced above, turbidite systems were initially classified following their sand richness (Reading and Richards, 1994), which has limitations in heterogeneous LBs observed in large systems (Piper and Normark, 2001). Fortunately, this NTG classification also gives the ranges of each system size, which can be applied to analyse the dimensions of their LBs. Consequently, three system sizes can be considered: large, medium, and small. They respectively correspond to the former mud-rich, mud/sand-rich, and sand-rich classes. Lobes are deposited in an environment corresponding to the middle-lower fan (Normark, 1970). In small systems, this environment is < 100 km-long, it is 100-300 km-long in

intermediate systems, and > 300 km-long in large systems. For simplicity, medium and large systems were merged into one category (i.e., large systems).

Some simplifications have been made to improve the representativeness and the consistency of the LB classes. They are described below. For more details about each turbidite system, please refer to SM or to source studies.

First, some changes were made based on groups of LBs that exhibit dimensions that are characteristics of another class of system. LBs from well-known "large" systems come from the Amazon, Congo, Mississippi, and Nile systems (n = 106). Similarly, the LBs from the Rhône fan, Rhone Neofan, Celtic fan (n = 17), which are described as mud/sand-rich systems (Droz et al., 2020; Reading and Richards, 1994; Zaragosi et al., 2003), but also from the Monterey (Fildani and Normark, 2004) and Bering Sea fans (Kenyon and Millington, 1995) (n = 8) would correspond to medium-sized systems. Therefore, they were classified as part of the large systems (SM) category.

Second, intraslope LBs, which are described as sandy and small in the literature, were added into the small systems class because intraslope basins create segmented sub-basins within turbidite systems that can evolve diachronously from up- to down-slope (Prather, 2020; Prather et al., 2012). This included (SM): the intraslope H3 of the Nile system (Shi et al., 2021), the intraslope H2-H4 of the Niger Delta (Jobe et al., 2017; Pizzi et al., 2023; Prather et al., 2012; Zhang et al., 2016) and the basin floor H3 of the Niger Delta (Prélat et al., 2010; Zhang et al., 2016). Finally, on the same basis, LBs (n = 3) of three coarse-grained systems (database) were also added to the small systems class.

2.2. Measurements and calculated dimensions

Three morphological attributes were measured for LBs based on facies boundaries and stratal onlaps/downlaps: 1) the down-flow length (L), 2) the maximum width (W), and 3) the maximum thickness (H) (Fig. 3). Length was measured from the apex of the lobe located downdip of the channel-mouth, which constitutes a more-or-less diffuse transition zone dominated by sediment bypass (Bonnel et al., 2005; Droz et al., 2020; Wynn et al., 2002), to the distal fringe. Maximum width was measured perpendicularly to the length, and maximum thickness was estimated from 2D section(s) where the thickness scale was available in meters or when vertical exaggeration was indicated (Fig. 3).

Both planform and vertical delimitation of LBs depend on the data resolution. In the case of datasets acquired with side-scan sonar, sub-bottom profiles and acoustics, measurement of thickness was often limited by vertical resolution and/or source penetration (10 to 40 m). Unfortunately, this resulted in series of constant thickness values for some LBs from the Amazon, Al Batha, Gulf of Cadiz, Mississippi, Nile, and Rhone systems (database). The number of data where the thickness of LBs is known is thus smaller (n = 307) than the number of data where the planform dimensions are known (n

= 365). Planform delimitation may somehow be interpretative due to a gradual facies transition (Pettinga et al., 2018) on sonar and seismic attribute maps (Fig. 3). We thus (re)measured as accurately as possible the planform dimensions of LBs with a GIS software within the systems of modern Amazon (Jegou et al., 2008), modern Congo (Dennielou et al., 2017), Kutai Basin (Saller et al., 2008), and Brazos-Trinity Basin IV upper sequence (Beaubouef et al., 2003).

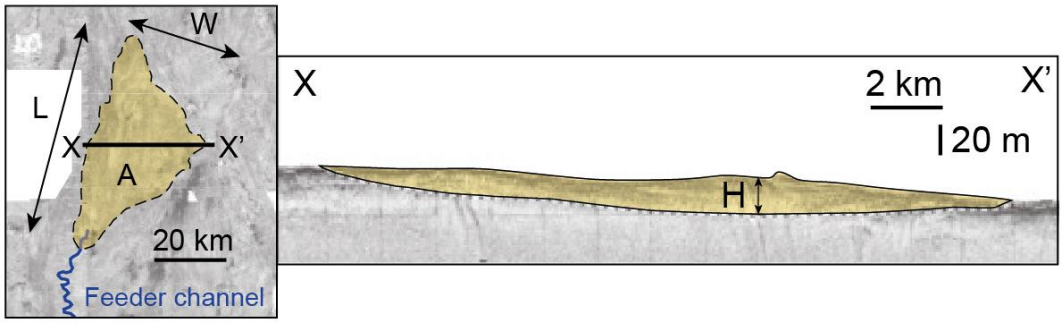

Figure 3. Example of measurements made from sonar and seismic data: lobe body length (L), width (W), thickness (H), and area (modified after Jegou et al., 2008; Pettinga et al., 2018).

Usually, area (A) and volume (V) of LBs are not measured by authors. They can be calculated using the following ellipsoid equations (Prélat et al., 2009):

$$A = \pi \frac{L}{2} \frac{W}{2} = \frac{1}{4} \pi L W \quad \text{(eq1)}$$

$$V = \frac{4}{3} \pi \frac{L}{2} \frac{W}{2} \frac{H}{2} = \frac{1}{6} \pi L W H \quad \text{(eq2)}$$

Sometimes, the area was measured in the literature or digitized on maps (systems listed above). Only the volume was then calculated using *equation 2*. Note that due to variations in LB morphology, a ≈ 25% error is found between measured and calculated values of area and volume (Pettinga et al., 2018).

The measured and calculated dimensions were used to compare length vs. width (Fig. 4), to show the distribution of the size of the different LBs (Fig. 5), and to follow the evolution of the thickness-to-area ratio with hierarchy (Fig. 6). Finally, we also established morphometric scaling relationships between the length and the width-to-thickness ratio (Fig. 7).

3. Results

3.1. Shape similarities between lobe bodies

A considerable overlap of the median elongation ratio (i.e., L/W) of architectural levels is observed for marine LBs (Figs. 4, 5A). When considering the whole dataset, the width and length of marine LBs scale linearly, with a planform aspect ratio close to 2:

$L = 1.94*W$, $r^2 = 0.85$, $n = 370$ (Fig. 4). (eq3)

This ratio is higher than the one proposed by Pettinga et al. (2018) for a similar correlation factor (i.e., $L \approx 1.7*W$, $r^2 = 0.86$, $n = 271$).

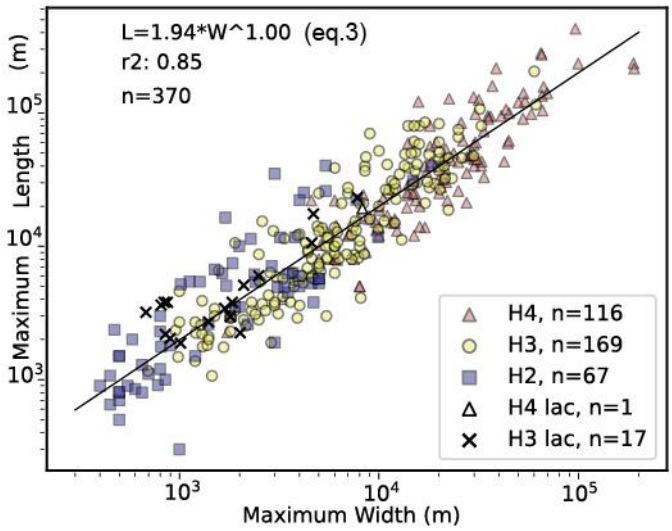

Figure 4. Scaling relationship for lobe bodies where length correlates to width (modified after Pettinga et al., 2018). Hierarchical levels of distal lobe bodies are lobe element (H2), lobe (H3), and lobe complex (H4). H3lac and H4lac, respectively, refer to lacustrine lobe and lobe complex.

3.2. Influence of hierarchical level for marine LBs

3.2.1. Dimensions

In detail, the elongation ratio of LBs is different depending on their hierarchical levels (Figs 5A, Tab. 1). Lobe elements (H2) have the greatest elongation ratio (i.e., 1.98) and lobe complexes (H4) the smallest (i.e., 1.71), while H3 have an intermediate L/W ratio (i.e., 1.89). Note that H2 also show the greater dispersion of L/W ratio from quartiles Q1 to Q3, while H4 exhibit the smallest dispersion from the first (Q1) to the third (Q3) quartile (Fig. 5A).

When considering the Q1-Q3 interval, hierarchical levels of marine LBs can be well individualized based on their maximum thickness. Indeed, the limit between H2 and H3 is ca. 10 m while the limit between H3 and H4 is ca. 40 m (Fig. 5B). H2 have a median thickness of 6.7 m, H3 of 22 m, and H4 of 75.6 m. Moreover, note that H3 have the greatest Q1-Q3 range of maximum thickness values among LBs (Fig. 5B).

The area of marine LBs (both median and mean values) increases by one order of magnitude when hierarchy increases, with a median area of 5.7 km^2 for H2, ca. 50 km^2 for H3, and ca. 650 km^2 for H4 (Fig. 5C). The median volume of marine LBs increases by more than one order of magnitude (about 30

to 40 times) between two successive hierarchical levels: it is 1.8 x10^{-2} km^3 for H2, 7.17 x10^{-1} km^3 for H3 and 31.3 km^3 for H4 (Fig. 5D).

Hn	System type	n	Stat	L (m)	W (m)	H* (m)	A (km^2)	V* (km^3)	L/W
H2	Undifferenciated	67	P50	4950	1800	6.7	5.68	1.80E-02	1.98
		65*	Mean	7273	2711	7.5	23.4	5.70E-02	2.72
	Small systems	57	P50	3000	1400	8.4	3.75	1.29E-02	1.75
		55*	Mean	3811	1882	8.6	6.92	3.65E-02	2.26
	Large systems	10	P50	25650	5400	1.5	91.5	1.01E-01	5.18
		10*	Mean	27010	7440	1.5	117.0	1.70E-01	5.35
H3	Undifferenciated	169	P50	11419	6000	23.2	49.8	7.17E-01	1.89
		133*	Mean	21967	9053	22.0	281.1	2.07	2.27
	Small systems	117	P50	6574	4170	25.0	23.6	3.83E-01	1.67
		95*	Mean	9436	5482	24.2	64.7	6.35E-01	1.85
	Large systems	52	P50	41150	15083	15.0	470.0	5.12	2.87
		33*	Mean	50162	17089	15.9	767.9	6.19	3.21
H4	Undifferenciated	115	P50	40000	20900	76.5	646.0	31.3	1.71
		96*	Mean	60439	27978	81.3	2109	64.4	2.07
	Small systems	46	P50	15100	10000	75.0	113.5	5.3	1.35
		35*	Mean	18413	12325	95.0	201.3	9.16	1.58
	Large systems	69	P50	59400	29800	78.0	1160.0	57.0	2.05
		61*	Mean	88456	38412	73.5	3380.0	96.1	2.40
H3 lac.	Lacustrine lobes	17	P50	3620	1690	6.9	3.26	9.00E-03	2.40
		17*	Mean	5768	2142	13.1	17.5	2.20E-01	2.79

Table 1: Median (P50) and mean dimensions of lobe bodies in function of their hierarchy and system size. Hierarchical levels are lobe element (H2), lobe (H3), lobe complex (H4), and lacustrine lobe (H3lac).

3.2.2. Thickness-to-area trends

Evolution of the thickness-to-area ratio is a way to consider shaping of LBs with hierarchy (Pettinga et al., 2018; Straub and Pyles, 2012). Two trends (i.e., “trend 1” and “trend 2”), which spread over at least two hierarchical levels, may be tentatively represented when considering the whole dataset (Fig. 6A). In details, some systems align perfectly with these trends (Figs. 6B). For instance, the Kutai, Myanmar and East Corsica systems fit well with trend 1 while the Mississippi and Al Batha can be considered to follow trend 2. On the contrary, the Karoo system, which has been computed from outcrops, seems to start close to trend 1 and then to follow trend 2. Then, the LBs from the modern Congo show an evolution which is different from trend 2 (Figs. 6B, 6D), and the LBs from the Nigeria intraslope system do not evolve following trend 1 (Figs. 6B, 6C). Therefore, systems respectively belonging to each trend show an increase both in area and in thickness, which operates between each hierarchical level, and also in each system type (Figs. 6C, 6D). However, variations in thickness and area may vary between systems and between hierarchical levels (Figs. 6C, 6D).

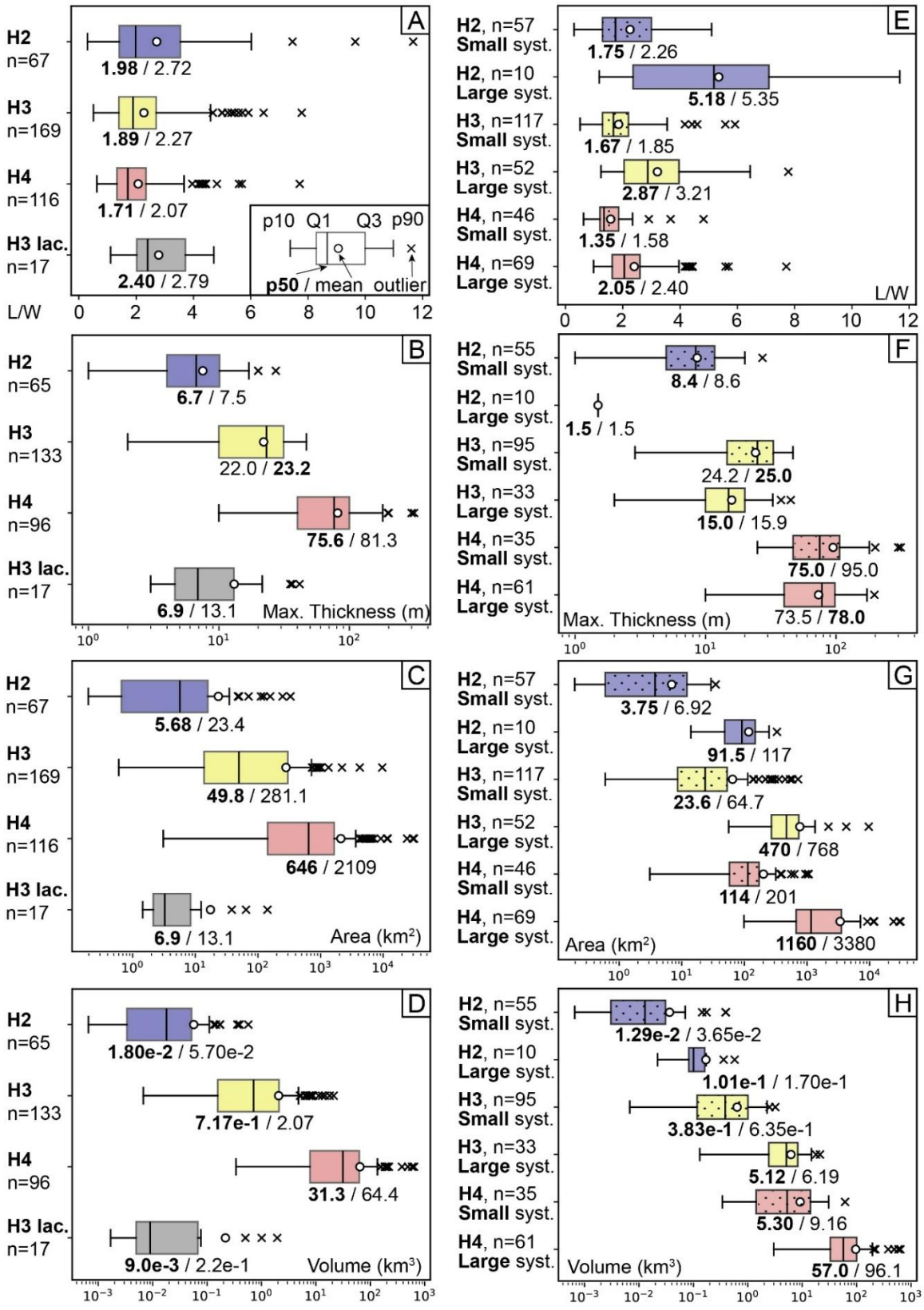

Figure 5. Boxplot diagrams of some lobe bodies. A: Length-to-width ratio by hierarchy. B: Thickness by hierarchy. C: Area by hierarchy. D: Volume by hierarchy. E: Length-to-width ratio by hierarchy and system size. F: Thickness by hierarchy and system size. G: Area by hierarchy and system size. H: Volume by hierarchy and system type. Hierarchical levels of distal lobe bodies are lobe element (H2), lobe (H3), lobe complex (H4), and lacustrine lobe (H3lac). Keys of statistics are provided in Figure 5A.

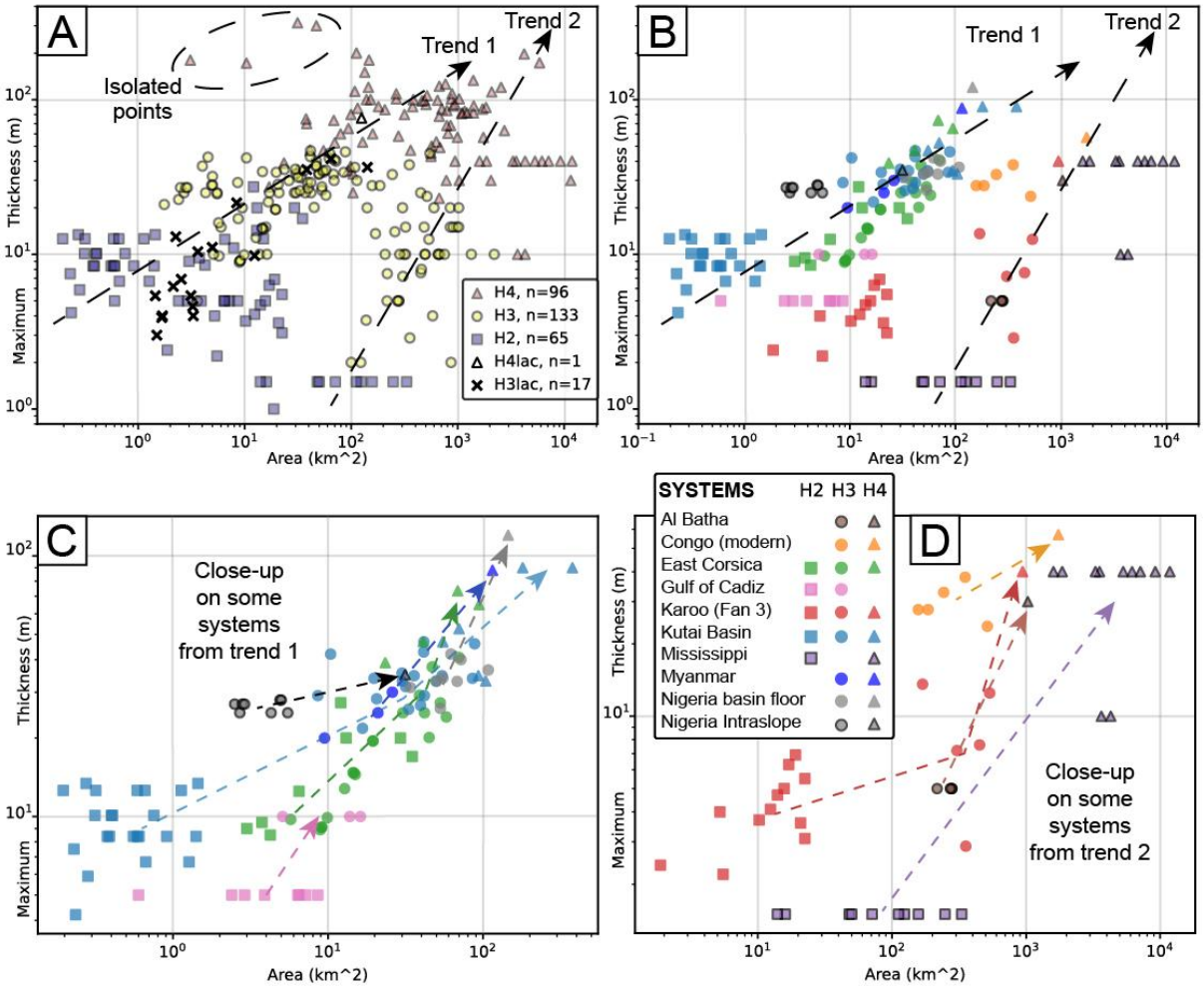

Figure 6. Thickness vs. area plots. A: Trends of evolution through hierarchical levels, "trend 1" for instance fits with "confined" lobe bodies, and "trend 2' fits with "unconfined" lobe bodies (modified after Pettinga et al. 2018). B: some selected systems that belong to "trend 1" and "trend 2". C: Close-up on some systems from to "trend 1". D: Close-up on some systems from to "trend 2".

3.2.3. 3D scaling relationships

A correlation is found between the length of LBs and their width/thickness ratio (Fig. 7A).

$L = 272*(W/H)^{0.67}$, $r^2 = 0.39$; n = 307, (Fig. 7A). (eq4)

When considering all the data, the coefficient of the regression is weak ($r^2 \approx 0.39$). But when considering data from one hierarchical level only, the coefficients of the regression are clearly better ($r^2 \approx 0.69$; Fig. 7B). This indicates that each hierarchical level has a distinct scaling relationship (Fig. 7B):

_ H2 i.e. lobe elements, $L = 94.59*(W/H)^{0.64}$, $r^2 = 0.69$, n = 65, (eq5)

_ H3 i.e. lobes, $L = 211.78*(W/H)^{0.70}$, $r^2 = 0.69$, n = 133, (eq6)

_ H4 i.e. lobe complexes, $L = 558.62*(W/H)^{0.74}$, $r^2 = 0.69$, n = 96. (eq7)

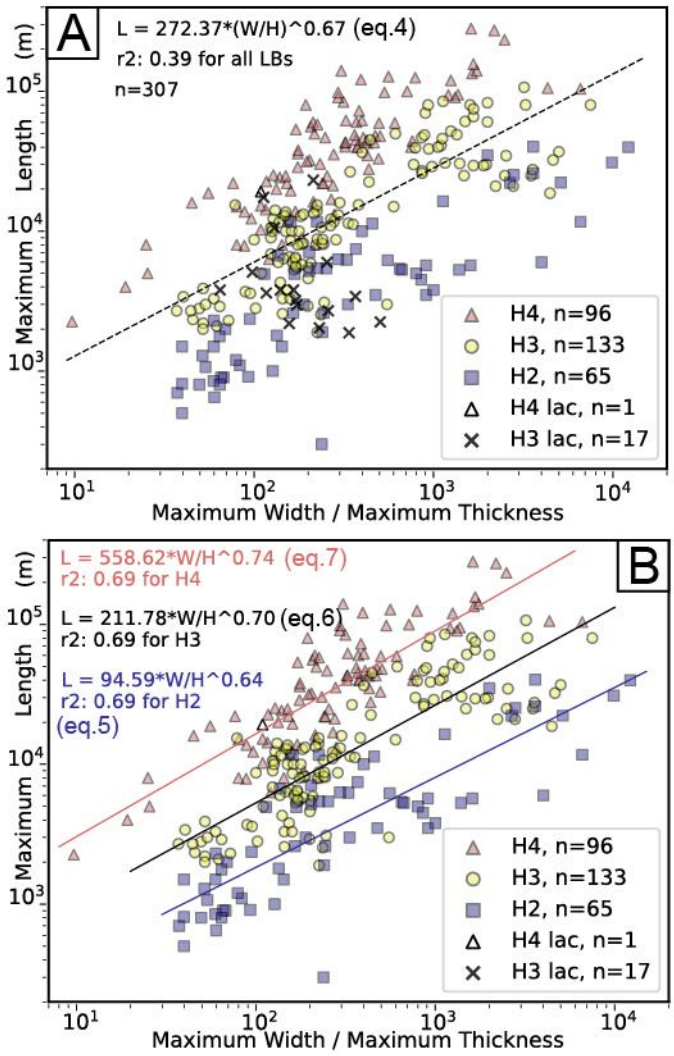

Figure 7. Scaling relationships for lobe bodies where length correlates to the thickness-to-area ratio. A: considering all the lobe bodies (LBs). B: considering independently each hierarchical level of exclusively marine lobe bodies, i.e., lobe element (H2), lobe (H3), and lobe complex (H4). H3lac and H4lac, respectively, refer to lacustrine lobe and lobe complex.

3.3. Comparison of marine LBs from small vs. large systems

In the following section, LBs belonging to different system size classes (i.e., small vs. large) are compared at an identical hierarchical level. Note that the comparison for H2 is limited by the small number of LBs (n = 10) in large systems (i.e., the modern Mississippi system only). LBs of large systems are often observed in unconfined settings (i.e., "trend 2"), while LBs of small systems are often deposited in confined settings (i.e., "trend 1") (Fig. 6A). One source of bias when comparing LBs from small vs. large systems is the potential for topographic confinement, which may occur in some settings and can reduce LBs area while increasing LBs thickness(Pettinga et al., 2018; Prélat et al., 2010).

The elongation (L/W) ratio is different between LBs from small and large systems. LBs from large systems exhibit a greater elongation ratio than LBs from small systems, which is verified at each hierarchical level (Fig. 5E). Indeed, LBs from large systems have a median elongation ratio above 2,

while LBs from small systems have a median elongation ratio below 2. Therefore, one should note that lobe elements from large systems have the greater median elongation ratio (ca. 5). When considering all system types, the elongation ratio decreases with increasing hierarchy (Fig 5E). In large systems, a consistent decrease of the elongation ratio with increasing hierarchy is observed. In small systems, H2 are slightly more elongated (median L/W ratio = 1.75) than H3 (median L/W ratio = 1.67). H4 are more circular, with a median L/W ratio = 1.35 (Fig. 5E).

The area of LBs from large systems is one order of magnitude greater than the area of LBs from small systems (Fig. 5G). On the contrary, the thickness of LBs of small systems is greater than the thickness of LBs of large systems for H2 and H3. For H4, LBs from small and large systems have the same median thickness of about 75 m (Fig. 5F).

Finally, at each hierarchical level, the volume of LBs from large systems is at least one order of magnitude greater than the volume of LBs from small systems (Fig. 5H). Therefore, at the scale of lobes (H3), the median volume is ≈ 0.4 km^3 in small systems, while the median volume is ≈ 5 km^3 in large systems. Finally, data show that the volume of LBs increases by at least one order of magnitude when hierarchy increases for both small and large systems (Fig. 5H).

3.4. Comparison between marine LBs and lacustrine lobes

Lacustrine LBs (H3 mainly reported, i.e., n = 17 with only n = 1 for H4) represent a distinctive group from both their deposition environment and their dimensions. They are more elongated than most of the marine LBs from small systems (i.e., median L/W ratio = 2.40) (Fig. 5A). Their elongated shape is well defined in the ancient systems from the North Falkland Basin (Dodd et al., 2019), from the Niuzhang Sag of Eastern China (Shi et al., 2021), or from the modern Geneva Lake (Silva et al., 2019). Moreover, lacustrine H3 show planform dimensions (length and width, Tab. 1; thickness, Fig. 5C) and size (area and volume, Figs 5C, 5D, Tab. 1) close to those exhibited by marine H2. Thus, lacustrine H3 are usually much smaller than marine H3, which is also visible on the thickness-to-area plot (Fig. 6).

4. Discussion

4.1. Volumes

4.1.1. Disparities between hierarchical levels

Our results show that the volume of LBs increases by one order of magnitude at each hierarchical level (Fig. 5D). These results are in agreement with previous studies that introduced notions of hierarchy (Pettinga et al., 2018; Prélat et al., 2010) and that highlighted that the principal criterion of distinction between hierarchical levels is the volume (Fig. 5D). This supports that H3 and H4 are usually composed

of about ten LBs of inferior scale. A reason of this volume partitioning may be that feeder channels are also ordered by size (Pickering et al., 2015; Pickering and Clark, 1996), i.e., from channel complexes (largest) to storeys or distributaries (smallest), where dimensions of the channel section strongly correlate with the volume of the associated terminal LBs (Pettinga et al., 2018). Finally, one should note that the mean volume of H3 found in our study is ≈ 2 km^3 (i.e., 2.07 km^3), which is slightly less than previously described by Pettinga et al. (2018), i.e., 2.9 km^3. The reason is that our study included intraslope LBs, which usually have smaller volumes than basin floor LBs (database, Pettinga et al. 2018).

4.1.2. Heterogeneity of LBs between system types

A new finding of this study is that the volume of LBs depends on the system type they belong to, i.e., LBs of small systems are composed of smaller LBs than those belonging to large systems (Figs. 5H, 8). Indeed, by comparing LBs of the same hierarchical level, we show that LBs from large systems are usually one order of magnitude more voluminous than LBs from small systems (Fig. 5H). Therefore, in addition to having the longest feeder channels (Curray et al., 2002; Jegou et al., 2008; Migeon et al., 2010; Picot et al., 2016; Twichell et al., 2009), large turbidite systems also host the most voluminous LBs at every hierarchical level (Fig. 5H, 8). These findings are in contradiction with the interpretation of Prélat et al. 2010 that assumed a similar mean volume of lobes (i.e., ≈ 2 km^3) independently of the basin settings. Using the present dataset, it was not possible to find a correlation between the dimensions of LBs and those of their terrestrial feeding systems. This lack of correlation is in agreement with previous findings (Pettinga et al., 2018; Romans et al., 2016), and suggests that some degree of self-organization does exist in the construction of submarine LBs.

Other parameters may control LBs volume, such as regional slope gradient and transport distance (Sømme et al., 2009). The latter process progressively filters out the turbidite record of high-frequency and small-volume events (Allin et al., 2017; Jobe et al., 2018; Talling, 2014). Nevertheless, medium (i.e., Rhône) and large systems (i.e., Amazon, Congo, Mississippi, Nile) present the most voluminous LBs, meaning that transport distance is not a strong limiting factor to the amount of material deposited in terminal LBs. In large systems, voluminous turbiditic flows may be able to run long distances (Allin et al., 2017; Jobe et al., 2018; Talling et al., 2022). The process-based classification of deep-sea fans (Piper and Normark, 2001) established that large, passive-margin rivers deliver sand and mud generated by load-induced slumping of rapidly prograding deltaic sediments (e.g., Amazon, Indus, and Rhône systems) that generate voluminous turbiditic flows (Talling, 2014). Following this process-based classification, the Rhône system consequently operates as a large system, which is coherent with the volume of its lobes being close to that of large systems (i.e., often > 2 km^3) (database, Fig. 5H). Although each sedimentary system has its specificities (Romans et al., 2016), such large systems usually provide

the most stable depositional conditions (i.e., flow volume, frequency, and type), especially during sea level lowstands (Piper and Normark, 2001). Additionally, river-fed canyons such as the Congo are flushed every few years by powerful and long run-out flows (Talling, 2014; Talling et al., 2022), leading to relatively regular and voluminous deposition in these deep-sea fans (Picot et al., 2019, 2016).

On the contrary, sea-level variations may more strongly influence small systems in response: (1) to hyperpycnal currents and delta-front slumping (Gervais et al., 2006; Piper and Normark, 2001), (2) to active/inactive shelf processes that promote sourcing of different particle size (Piper and Normark, 2009; Talling, 2014; Zaragosi et al., 2003), (3) to subaerial exposition of the shelf during sea-level lowstands (Romans et al., 2016) and (4) to more variability in the frequency and intensity of flushing events (Allin et al., 2017; Jobe et al., 2018; Talling, 2014). On the one hand, these variations, together with the limited sediment supply (Romans et al., 2016; Sømme et al., 2009; Syvitski and Milliman, 2007), lead to less frequent and more heterogeneous deposition in small systems, and thus to less voluminous LBs (Fig. 5H, 8). On the other hand, some small systems occasionally contain lobes (H3) with volumes comparable to those formed by large systems (> 1 km^3, Figs 5H). Usually, this may be due to the efficient bypass of sediment from catchment to deep environments in small systems (Sømme et al., 2009). In this study, these small systems, where the source-to-sink routing is better known (i.e., in Pleistocene systems), belong to the Brazos-Trinity Basin II and Basin IV, and to the Kutai Basin Fan (database). Indeed, each of these previously cited systems shows coarse-grained feeding of its fan associated with subaerial shelf exposure and/or intense channelization of the shelf edge (Romans et al., 2016; Saller et al., 2008).

4.1.3. Heterogeneity of LBs between "large" systems

Our dataset shows that lobe volume is also heterogeneous within large systems (database). The most voluminous lobes are deposited within the Congo and Rhône, where they often reach 5-10 km^3 (database), while the Amazon lobes are less voluminous (≈ 2-5 km^3) (database). These differences arise from different source-to-sink contexts.

The Congo fan is composed of voluminous lobes (database) because: (1) progradation phases are mainly controlled by West African Moonsoon within its large feeding catchment (Picot et al., 2016; Sømme et al., 2009) and less so by sea-level variations (Picot et al., 2019), (2) river-(submarine)canyon connection occurs even during highstands (Picot et al., 2019; Talling et al., 2022), and (3) floods generate strong erosional turbidity currents that can accelerate thereby travelling much further (Talling et al., 2022). During sea-level lowstands, the Rhône fan has similarities with the Congo fan, despite being mainly fed by Alpine catchments. There, an efficient river-canyon connection occurred during Late Pleistocene lowstands via a deep incised valley, until the onset of the post-glacial sea-level rise (Droz et al., 2020, and references therein). Furthermore, the Rhône system has a moderate length that minimizes

sediment storage in turbidite channels. In the Amazon system, the sediment supply depends on the distance between the source and the canyon head on a particularly wide shelf. This distance depends on (1) climatic conditions within the drainage basin, and (2) sea-level variations that control delta migration and shelf currents (Jegou et al., 2008). Therefore, even during sea-level lowstands, the river-canyon connection appears to be much less effective in the Amazon than in the Congo and Rhône systems, influencing the amount of sediment transported to deep environments.

4.1.4. Small volume of lacustrine lobes

The small volume of lacustrine H3 is close to that of marine H2 (Fig. 5F). This is likely the result of the location of lacustrine LBs along the sediment routing system: they are fed by smaller drainages than marine systems. However, these findings must be taken with caution as their volume varies a lot depending on the system (Fig. 5F) and as their 3D shape can be either close to that of marine H3 or even H4 (Fig. 7B). Currently, the limited amount of data available (n = 17) prevents further interpretation of the 3D shape of lacustrine LBs.

4.2. Influence of the system type on planform shape

From a 2D planform point of view, this study confirms that a lobe body is controlled by turbidity flows and exhibits an elongation ratio of about 2 in the median case (Fig. 4) (Pettinga et al., 2018). When looking into details, some differences can also be highlighted based on hierarchical order and system type. As a general comment, one must notice that the lobe elements (H2) of large systems (n = 10) only come from the recent Mississippi system, which is likely not fully representative.

4.2.1. Elongated LBs in marine environments

The greater elongation (L/W) ratio observed for LBs within large systems (Figs. 5E, 8) may be due to several factors. First, erosive turbidity currents have the capacity to accelerate and thus to run long distances, as observed in the Congo (Talling et al., 2022). Thus, within large systems where gravity flows are potentially more voluminous, high flow discharge can create more elongated deposits (Spychala et al 2020) and enhance progradation (Spychala et al., 2020; Ferguson et al., 2020).

Second, in large systems, debris-flows frequently reach the abyssal environment: they were observed in the Mississippi (Schwab et al., 1996; Talling et al., 2010; Twichell et al., 2009), Nile (Migeon et al., 2010), and Congo (Dennielou et al., 2017) systems. Debrites are usually elongated deposits (Goodwin and Prior, 1989; Haughton et al., 2009; Talling et al., 2010). Within the Mississippi and Nile systems, debrites and hybrid-bed events constitute “frond-like” or “finger-like” LBs with a

dendritic pattern (Haughton et al., 2009; Migeon et al., 2010; Schwab et al., 1996; Talling et al., 2010; Twichell et al., 2009). Although cohesive flows are not the main depositional process operating within the Mississippi, some LBs are mainly constructed by hybrid and turbulent flows (Fildani et al., 2018). These LBs constitute ≈ 5-20 m-thick units (i.e., lobe elements and lobes) of hybrid-event beds, which are mainly composed of poorly sorted fine-to-medium grained sand within a matrix of silt and mud, or sandy mud (Fildani et al., 2018). Similar "dirty" sands are also observed within the lobe fringes of the Congo system, while distributary channels are plugged by sandy debrites (Dennielou et al., 2017). Similarly, the relatively small-sized Al Batha system is composed of finger-like and sand-rich lobes, whose axes are mainly composed of bipartite massive beds (sandy debrites topped by fine-sand beds), resulting from concentrated flows generated during hyperpycnal events (Bourget et al., 2010).

Therefore, the mud fraction of cohesive/liquified flows or hybrid flows seems to greatly contribute to the elongation of LBs within large systems (Fildani et al., 2018; Haughton et al., 2009; Migeon et al., 2010; Talling et al., 2010). Finally, in the Congo system, a transcritical flow regime is interpreted as the cause of elongated deposits at the larger (i.e., H4 to fan) scale (Wahab et al., 2022).

4.2.2. Elongated shape of lacustrine lobes

The elongated shape of lacustrine lobes (Figs. 5A, 8) may be related to the important contribution of hyperpycnal flows that operate in these environments (Dodd et al., 2019; Shi et al., 2021; Silva et al., 2019). Similar to marine systems, this kind of flows may produce high-density turbidity flows (Dodd et al., 2019; Shi et al., 2021; Silva et al., 2019) and hybrid events (Dodd et al., 2019). Therefore, in lacustrine environments, lobes can also show a frond-like pattern (Dodd et al., 2019), but their lobe axis and proximal fringe seem to be dominated by high-density turbidites, respectively of one-meter-thick to pluri-decimeter-thick, and hybrid beds seem to be negligible (Dodd et al., 2019; Shi et al., 2021). Thus, one can suppose that in such environments, high-density turbidity currents are sufficient to create a frond-like pattern.

4.2.3. Elongation limitation within small systems

Regarding small (sand-rich) systems, field studies (Postma and Kleverlaan, 2018; Rohais et al., 2021) and experimental ones (Hamilton et al., 2017) described lobe building in three distinct phases: 1) progradation, 2) aggradation, and sometimes 3) retrogradation (Fig. 1). This retrogradational phase is observed in the small systems of East Corsica (Deptuck et al., 2008; Sweet et al., 2019). Retrogradation is interpreted as a consequence of the frontal confinement and hydraulic jump of flows, due to the relief made by the aggradation of lobe elements deposited during phases 1 and 2 (Hamilton et al., 2017; Postma and Kleverlaan, 2018). Backstepping can also be the result of a flow discharge decrease at the end of

the lobe deposition (Ferguson et al., 2020), which is also suspected for the East Corsica lobes (Gervais et al., 2006). The combination of the two aforementioned processes, which are respectively autocyclic and allocyclic, may therefore limit lobe progradation and thus increase widening. To date, such architectural evolution has not been described in large systems.

Finally, the break of slope (i.e., from feeder channel to lobe depositional area) is more important in small systems than in large systems (Denneilou et al., 2017; Deptuck et al., 2008; Droz et al., 2020; Jegou et al., 2008; Prélat et al., 2010; Saller et al., 2008). The break of slope leads to thicker LBs (Pohl et al., 2020a) and particularly to thicker lobe elements (Fig. 5F). As a result, aggradation is enhanced during lobe building in small systems, favouring the formation of hydraulic jumping and the backstepping of the lobes (H3) (Hamilton et al., 2017; Postma and Kleverlaan, 2018). In small systems, thick lobe elements (H2) (Tab. 1) may also trigger more easily lateral compensation, thus participating directly in the widening of H3 (Figs. 1, 8). These processes thus lead to the reduction of the elongation ratio of the H3.

4.3. 3D change of LBs' morphology with hierarchy

4.3.1. Widening

The elongation ratio (L/W) of LBs decreases with hierarchy when considering all data: it is 2 for H2, 1.9 for H3, and 1.7 for H4 (Figs. 5A). Moreover, the same trend is observed when considering small and large systems independently (Figs. 5E, 8). This statistically supports that LBs are relatively wider with increasing hierarchy and length, whatever their system size (Figs. 5E, 7B, 8). The widening of LBs from H2 to H3 could be the consequence: 1) of the positive relief resulting from H2 stacking, which modifies hydraulic properties at the mouth of the H3 channel and promotes hydraulic jump then backstepping (Hamilton et al., 2017; Postma and Kleverlaan, 2018), and 2) of the variations of flow discharge through times, with a low discharge that enhances backstepping (Ferguson et al., 2020). Moreover, in large systems where the thickness of LBs is less important with respect to the depositional area (i.e., "trend 2" in Fig. 6), anterior topography (i.e., lobe axis-lobe fringe transition) may control the mouth location of the active channel, promoting flow deconfinement and lobe deposition, as observed in the modern lobe complex of the Congo system (Dennielou et al., 2017). In the same system, subcritical conditions (Wahab et al., 2022) also trigger channel bifurcations and therefore participate in spreading at several scales (Picot et al., 2016; Wahab et al., 2022).

Thus, these processes likely increase the radial distribution of lobes (H3) within lobe complexes (H4) by minimizing the longitudinal stacking of lobes. The low elongation ratio of H4 may result from a reduced progradation capacity of LBs, which operates from the scale of lobe elements up to the scale of lobe complexes.

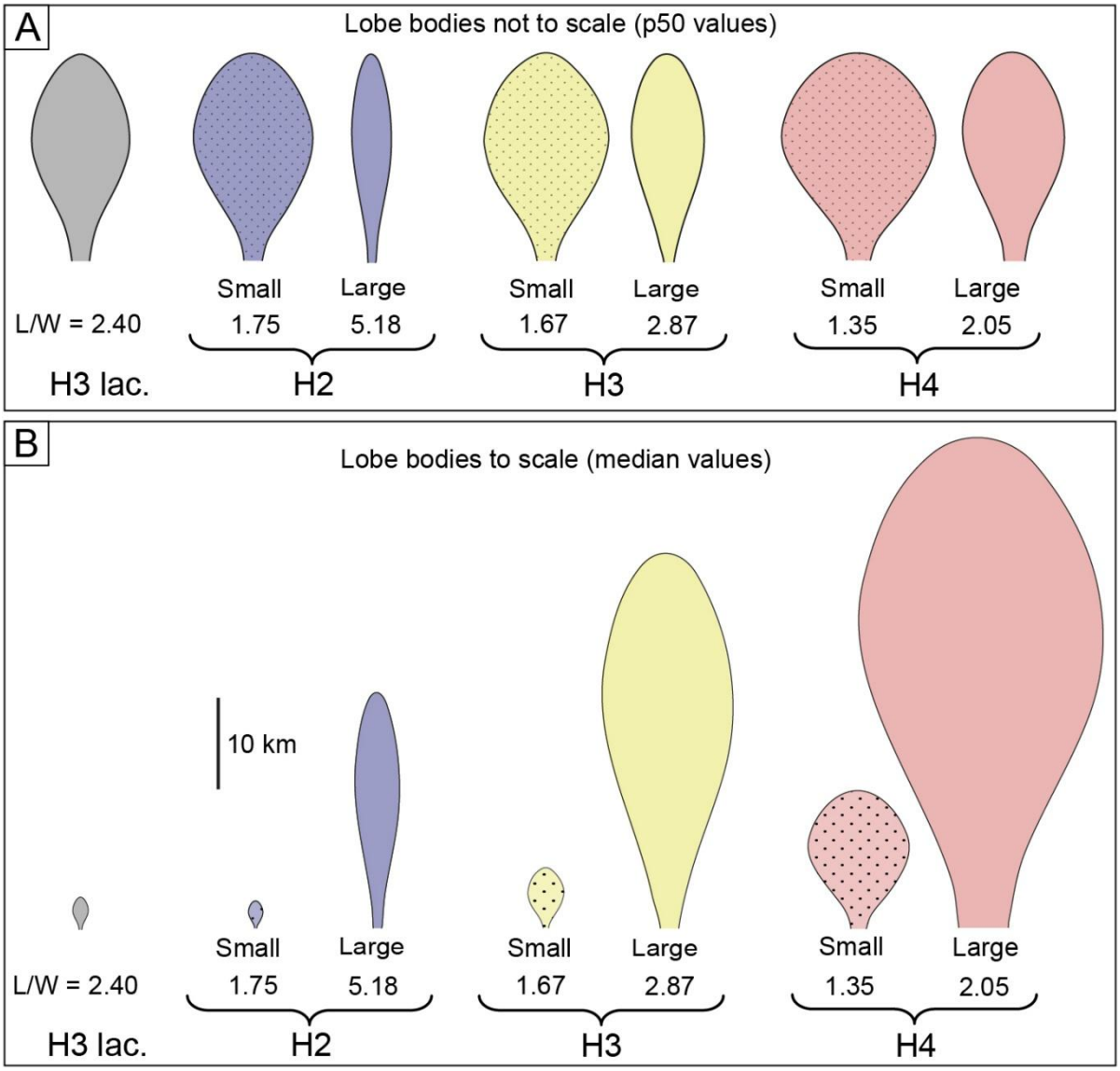

Figure 8. Schematic diagram of planform shapes and dimensions of lobe bodies considering the hierarchy and the system type. The compared hierarchical levels of lobe bodies are lobe element (H2), lobe (H3), lobe complex (H4), and lacustrine lobe (H3lac). The width of lobe bodies here is defined from the median length and median length/width ratio provided in Table 1.

4.3.2. 3D trends

H2, H3 and H4 have different 3D scaling relationships: length correlates differently with width-to-thickness ratio in each hierarchical level (Fig. 7B). At first glance, these relationships inform that, for a similar W/H ratio, H4 are longer than H3, which are longer than H2 (Fig. 7B). Another interpretation of these relationships is that for a similar length, H4 exhibit a smaller W/H ratio than H3, and H3 show a smaller W/H ratio than H4 (Fig. 7B). Factually, all these dimensions (i.e., length, width and thickness) increase with hierarchy (Figs. 4, 5B, 7B, Tab. 1). Thus, these trends show that, for each hierarchical level, the width-to-thickness ratio of LBs changes with length, because width increases comparatively

more than thickness. Therefore, when hierarchy increases, both length and W/H ratio increase (Fig. 7B), or conversely, the cross-section aspect ratio H/W decreases.

The above findings are thus consistent with the fact that LBs widen when their hierarchy increases (Figs. 5A, 8). Previous works suggested that the thickness-to-area of LBs decreases with hierarchy due to lateral stacking of LBs (Pettinga et al., 2018; Straub and Pyles, 2012). Some authors suggested that this process is effective for all systems of LBs (Straub and Pyles, 2012), while others suggested it is effective only for "confined" systems (i.e., the "trend 1" of Fig. 6A) (Pettinga et al., 2018). These authors argued that the H/A ratio decreases with hierarchy only for confined systems because they show a significant increase in area and a moderate increase in thickness (Fig. 6A, 7). Our study (database) allows us to compare area and thickness values between hierarchical levels in many different systems (Fig. 6B). A shift produced by a significant increase in area and a moderate increase in thickness is also observed, but it is effective for both "confined" (Fig. 6C) and "unconfined" (Fig. 6D) systems. This leads to a reduction in the thickness-to-area ratio as first suggested by Straub and Pyles, 2012. Furthermore, the three different scaling relationships identified in this study (Fig. 7B) confirm that each hierarchical level has a specific geometry and indicate a 3D change in shape that occurs in most systems. We nevertheless admit that quantifying the change of the shape in each system may be difficult due to the logarithmic representation of thickness vs. area values (Figs. 6B, 6C, 6D). It could also be difficult because the order of magnitude of changes may differ between systems, but also between the hierarchical levels of a system (Figs. 6C, 6D). Moreover, these changes do not follow mandatorily "trend 1" or "trend 2" (Fig. 6).

As discussed before, several processes are thus responsible for the widening of LBs. Progradation-retrogradation dynamics (Fig. 1) must also be considered for the construction of H3 and H4 (Dennielou et al., 2017; Deptuck et al., 2008; Gervais et al., 2006; Hamilton et al., 2017; Postma and Kleverlaan, 2018; Rohais et al., 2021; Sweet et al., 2019). These dynamics are primarily controlled by the volume of the flows (Allin et al., 2017; Deptuck et al., 2008; Ferguson et al., 2020) and by their regime (Hamilton et al., 2017; Postma and Kleverlaan, 2018; Rohais et al., 2021; Wahab et al., 2022). Finally, LBs thickness also increases -moderately- with hierarchy (Fig. 5D). Aggradation is due to overlapping of LBs as they build LBs of higher hierarchy (Fig. 1). This construction is due to 1) lateral compensation (Mutti and Normark, 1987; Straub and Pyles, 2012), 2) retrogradation that favours the cover of channel-lobe transition zones (Hamilton et al., 2017) and up-dip thickening (Deptuck et al., 2008), and 3) limited displacements or reoccupation of the feeder channel during avulsions (Saller et al., 2008; Dennielou et al., 2017; Picot et al., 2016) (Fig. 1).

Consequently, the 3D shape of LBs is controlled by autogenic and allogenic processes that promote the horizontal spreading of sediments, whereas vertical thickening appears secondary, largely as an indirect result of this complex superimposition of planar processes. This also suggests that

topographic confinement, which should increase the thickness of LBs by reducing their depositional area, is also a secondary process.

5. Conclusions

Our database thus illustrates how the size and shape of lobe bodies depend on hierarchy but also on system size. First, we show, as suggested by other studies, that the median planform shape of lobe bodies has an elongation ratio of 2. Second, hierarchy controls both the volume and the 3D shape of lobe bodies. We confirm that the volume roughly increases by one order of magnitude between two successive hierarchical levels, which can be used as a reliable criterion of distinction. We also demonstrate statistically that lobe bodies are less elongated with increasing hierarchy. Each hierarchical level exhibits a specific scaling relationship where length correlates with the thickness-to-width ratio. This change of 3D shape can be explained by the fact that systems, independently of their size, usually show a significant increase in area with increasing hierarchy, which is associated with an overall reduction of the thickness-to-area ratio. Third, lobe bodies from large systems are usually more elongated than those belonging to small systems. We also demonstrate statistically that for each hierarchical level, large systems produce lobe bodies that are one order of magnitude more voluminous than those of small systems, contrary to previous suppositions. Therefore, we consider that hierarchy is the first factor controlling the shape of lobe bodies, with system type having a significant influence on their volume and planform shape. Finally, we show that lacustrine lobes are one order less voluminous than marine lobes.

These evolving morphologies thus reflect the different modes of sediment dispersal into terminal lobes. Considering these morphological differences will help improve models of heterogeneities in deep-sea and deep lacustrine reservoirs and better assess the dispersal of pollutants such as microplastics and the burial of terrestrial carbon into the deep ocean.

References

Al Ja'Aidi, O.S., McCaffrey, W.D., Kneller, B.C., 2004. Factors influencing the deposit geometry of experimental turbidity currents: implications for sand-body architecture in confined basins. Geological Society, London, Special Publications 222, 45–58. https://doi.org/10.1144/GSL.SP.2004.222.01.04

Allan, J.R., Sun, S.Q., Trice, R., 2006. The deliberate search for the stratigraphic and subtle combination traps: where are we now?, in: The Deliberate Search for the Stratigraphic Trap, Geological Society London Special Publications. M.R. Allen, G.P. Goffrey, R.K Morgan & I.M. Walker, pp. 56–103.

Allin, J.R., Hunt, J.E., Clare, M.A., Talling, P.J., 2017. Eustatic sea-level controls on the flushing of a shelf-incising submarine canyon. GSA Bulletin 130, 222–237. https://doi.org/10.1130/B31658.1

Amy, L.A., 2019. A review of producing fields inferred to have upslope stratigraphically trapped turbidite reservoirs: Trapping styles (pure and combined), pinch-out formation, and depositional setting. AAPG Bulletin 103, 2861–2889. https://doi.org/10.1306/02251917408

Baas, J.H., Van Kesteren, W., Postma, G., 2004. Deposits of depletive high-density turbidity currents: a flume analogue of bed geometry, structure and texture. Sedimentology 51, 1053–1088. https://doi.org/10.1111/j.1365-3091.2004.00660.x

Beaubouef, R.T., Van Wagoner, J.C., Adair, N.L., 2003. Ultra-High Resolution 3-D Characterization of Deep-Water Deposits- II: Insights into the Evolution of a Submarine Fan and Comparisons with River Deltas*. Search and Discovery Article 8.

Bell, D., Soutter, E.L., Cumberpatch, Z.A., Ferguson, R.A., Spychala, Y.T., Kane, I.A., Eggenhuisen, J.T., 2021. Flow-process controls on grain type distribution in an experimental turbidity current deposit: Implications for detrital signal preservation and microplastic distribution in submarine fans. The Depositional Record 7, 392–415. https://doi.org/10.1002/dep2.153

Bonnel, C., Dennielou, B., Droz, L., Mulder, T., Berné, S., 2005. Architecture and depositional pattern of the Rhône Neofan and recent gravity activity in the Gulf of Lions (western Mediterranean). Marine and Petroleum Geology, The Gulf of Lions: an overview of recent studies within the French "Margins" Programme 22, 827–843. https://doi.org/10.1016/j.marpetgeo.2005.03.003

Bourget, J., Zaragosi, S., Mulder, T., Schneider, J.-L., Garlan, T., Van Toer, A., Mas, V., Ellouz-Zimmermann, N., 2010. Hyperpycnal-fed turbidite lobe architecture and recent sedimentary processes: A case study from the Al Batha turbidite system, Oman margin. Sedimentary Geology 229, 144–159. https://doi.org/10.1016/j.sedgeo.2009.03.009

Chen, P., Kane, I.A., Clare, M.A., Soutter, E.L., Mienis, F., Wogelius, R.A., Keavney, E., 2025. Direct Evidence That Microplastics Are Transported to the Deep Sea by Turbidity Currents. Environ. Sci. Technol. 59, 7278–7287. https://doi.org/10.1021/acs.est.4c12007

Curray, J.R., Emmel, F.J., Moore, D.G., 2002. The Bengal Fan: morphology, geometry, stratigraphy, history and processes. Marine and Petroleum Geology 19, 1191–1223. https://doi.org/10.1016/S0264-8172(03)00035-7

Dennielou, B., Droz, L., Babonneau, N., Jacq, C., Bonnel, C., Picot, M., Le Saout, M., Saout, Y., Bez, M., Savoye, B., Olu, K., Rabouille, C., 2017. Morphology, structure, composition and build-up processes of the active channel-mouth lobe complex of the Congo deep-sea fan with inputs from remotely operated underwater vehicle (ROV) multibeam and video surveys. Deep Sea Research Part II: Topical Studies in Oceanography, Organic carbon transfer and ecosystem functioning in the terminal lobes of the Congo deep-sea fan: The Conglobe multidisciplinary study 142, 25–49. https://doi.org/10.1016/j.dsr2.2017.03.010

Deptuck, M.E., Piper, D.J.W., Savoye, B., Gervais, A., 2008. Dimensions and architecture of late Pleistocene submarine lobes off the northern margin of East Corsica. Sedimentology 55, 869–898. https://doi.org/10.1111/j.1365-3091.2007.00926.x

Dodd, T.J.H., McCarthy, D.J., Richards, P.C., 2019. A depositional model for deep-lacustrine, partially confined, turbidite fans: Early Cretaceous, North Falkland Basin. Sedimentology 66, 53–80. https://doi.org/10.1111/sed.12483

Droz, L., Jégou, I., Gillet, H., Dennielou, B., Bez, M., Canals, M., Amblas, D., Lastras, G., Rabineau, M., 2020. On the termination of deep-sea fan channels: Examples from the Rhône Fan (Gulf of

Lion, Western Mediterranean Sea). Geomorphology 369, 107368. https://doi.org/10.1016/j.geomorph.2020.107368
Ferguson, R.A., Kane, I.A., Eggenhuisen, J.T., Pohl, F., Tilston, M., Spychala, Y.T., Brunt, R.L., 2020. Entangled external and internal controls on submarine fan evolution: an experimental perspective. The Depositional Record 6, 605–624. https://doi.org/10.1002/dep2.109
Fildani, A., Clark, J., Covault, J.A., Power, B., Romans, B.W., Aiello, I.W., 2018. Muddy sand and sandy mud on the distal Mississippi fan: Implications for lobe depositional processes. Geosphere 14, 1051–1066. https://doi.org/10.1130/GES01580.1
Fildani, A., Normark, W.R., 2004. Late Quaternary evolution of channel and lobe complexes of Monterey Fan. Marine Geology 206, 199–223. https://doi.org/10.1016/j.margeo.2004.03.001
Gervais, A., Savoye, B., Mulder, T., Gonthier, E., 2006. Sandy modern turbidite lobes: A new insight from high resolution seismic data. Marine and Petroleum Geology 23, 485–502. https://doi.org/10.1016/j.marpetgeo.2005.10.006
Goodwin, R.H., Prior, D.B., 1989. Geometry and depositional sequences of the Mississippi Canyon, Gulf of Mexico. Journal of Sedimentary Research 59, 318–329. https://doi.org/10.1306/212F8F85-2B24-11D7-8648000102C1865D
Hage, S., Baker, M.L., Babonneau, N., Soulet, G., Dennielou, B., Silva Jacinto, R., Hilton, R.G., Galy, V., Baudin, F., Rabouille, C., Vic, C., Sahin, S., Açikalin, S., Talling, P.J., 2024. How is particulate organic carbon transported through the river-fed submarine Congo Canyon to the deep sea? Biogeosciences 21, 4251–4272. https://doi.org/10.5194/bg-21-4251-2024
Hage, S., Galy, V.V., Cartigny, M.J.B., Heerema, C., Heijnen, M.S., Acikalin, S., Clare, M.A., Giesbrecht, I., Gröcke, D.R., Hendry, A., Hilton, R.G., Hubbard, S.M., Hunt, J.E., Lintern, D.G., McGhee, C., Parsons, D.R., Pope, E.L., Stacey, C.D., Sumner, E.J., Tank, S., Talling, P.J., 2022. Turbidity Currents Can Dictate Organic Carbon Fluxes Across River-Fed Fjords: An Example From Bute Inlet (BC, Canada) - Hage - 2022 - Journal of Geophysical Research: Biogeosciences - Wiley Online Library. Journal of Geophysical Research, Biogeociences 127, 16.
Hamilton, P., Gaillot, G., Strom, K., Fedele, J., Hoyal, D., 2017. Linking Hydraulic Properties In Supercritical Submarine Distributary Channels To Depositional-Lobe Geometry. Journal of Sedimentary Research 87, 935–950. https://doi.org/10.2110/jsr.2017.53
Haughton, P., Davis, C., McCaffrey, W., Barker, S., 2009. Hybrid sediment gravity flow deposits – Classification, origin and significance. Marine and Petroleum Geology, Sediment Gravity Flows - Recent Insights into their Dynamic and Stratified/Composite Nature 26, 1900–1918. https://doi.org/10.1016/j.marpetgeo.2009.02.012
Jegou, I., Savoye, B., Pirmez, C., Droz, L., 2008. Channel-mouth lobe complex of the recent Amazon Fan: The missing piece. Marine Geology 252, 62–77. https://doi.org/10.1016/j.margeo.2008.03.004
Jobe, Z.R., Howes, N., Romans, B.W., Covault, J.A., 2018. Volume and recurrence of submarine-fan-building turbidity current. The Depositional Record 4, 160–176. https://doi.org/10.1002/dep2.42
Jobe, Z.R., Sylvester, Z., Howes, N., Pirmez, C., Parker, A., Cantelli, A., Smith, R., Wolinsky, M.A., O'Byrne, C., Slowey, N., Prather, B., 2017. High-resolution, millennial-scale patterns of bed compensation on a sand-rich intraslope submarine fan, western Niger Delta slope. GSA Bulletin 129, 23–37. https://doi.org/10.1130/B31440.1
Kane, I.A., Clare, M.A., 2019. Dispersion, Accumulation, and the Ultimate Fate of Microplastics in Deep-Marine Environments: A Review and Future Directions. Front. Earth Sci. 7. https://doi.org/10.3389/feart.2019.00080
Kenyon, N.H., Millington, J., 1995. Contrasting deep-sea depositional systems in the Bering Sea, in: Pickering, K.T., Hiscott, R.N., Kenyon, N.H., Ricci Lucchi, F., Smith, R.D.A. (Eds.), Atlas of Deep Water Environments: Architectural Style in Turbidite Systems. Springer Netherlands, Dordrecht, pp. 196–202. https://doi.org/10.1007/978-94-011-1234-5_28
Migeon, S., Ducassou, E., Le Gonidec, Y., Rouillard, P., Mascle, J., Revel-Rolland, M., 2010. Lobe construction and sand/mud segregation by turbidity currents and debris flows on the western Nile deep-sea fan (Eastern Mediterranean). Sedimentary Geology, Lobes in deep-sea turbidite systems 229, 124–143. https://doi.org/10.1016/j.sedgeo.2010.02.011

Mutti, E., Normark, W.R., 1987. Comparing Examples of Modern and Ancient Turbidite Systems: Problems and Concepts, in: Leggett, J.K., Zuffa, G.G. (Eds.), Marine Clastic Sedimentology: Concepts and Case Studies. Springer Netherlands, Dordrecht, pp. 1–38. https://doi.org/10.1007/978-94-009-3241-8_1

Normark, W.R., 1970. Growth Patterns of Deep-Sea Fans1. AAPG Bulletin 54, 2170–2195. https://doi.org/10.1306/5D25CC79-16C1-11D7-8645000102C1865D

Pettinga, L., Jobe, Z., Shumaker, L., Howes, N., 2018. Morphometric scaling relationships in submarine channel–lobe systems. Geology 46, 819–822. https://doi.org/10.1130/G45142.1

Pickering, K.T., Clark, J.D., 1996. Architectural Elements and Growth Patterns of Submarine Channels: Application to Hydrocarbon Exploration1. AAPG Bulletin 80, 194–220. https://doi.org/10.1306/64ED878C-1724-11D7-8645000102C1865D

Pickering, K.T., Corregidor, J., Clark, J.D., 2015. Architecture and stacking patterns of lower-slope and proximal basin-floor channelised submarine fans, Middle Eocene Ainsa System, Spanish Pyrenees: An integrated outcrop–subsurface study. Earth-Science Reviews, Deep-marine systems, Eocene Upper Hecho Group, Ainsa Basin, Spanish Pyrenees 144, 47–81. https://doi.org/10.1016/j.earscirev.2014.11.017

Picot, M., Droz, L., Marsset, T., Dennielou, B., Bez, M., 2016. Controls on turbidite sedimentation: Insights from a quantitative approach of submarine channel and lobe architecture (Late Quaternary Congo Fan). Marine and Petroleum Geology 72, 423–446. https://doi.org/10.1016/j.marpetgeo.2016.02.004

Picot, M., Marsset, T., Droz, L., Dennielou, B., Baudin, F., Hermoso, M., de Rafelis, M., Sionneau, T., Cremer, M., Laurent, D., Bez, M., 2019. Monsoon control on channel avulsions in the Late Quaternary Congo Fan. Quaternary Science Reviews 204, 149–171. https://doi.org/10.1016/j.quascirev.2018.11.033

Piper, D.J.W., Normark, W.R., 2009. Processes That Initiate Turbidity Currents and Their Influence on Turbidites: A Marine Geology Perspective. Journal of Sedimentary Research 79, 347–362. https://doi.org/10.2110/jsr.2009.046

Piper, D.J.W., Normark, W.R., 2001. Sandy Fans-From Amazon to Hueneme and Beyond. AAPG Bulletin 85, 1407–1438. https://doi.org/10.1306/8626CACD-173B-11D7-8645000102C1865D

Pizzi, M., Whittaker, A.C., Mayall, M., Lonergan, L., 2023. Structural controls on the pathways and sedimentary architecture of submarine channels: New constraints from the Niger Delta. Basin Research 35, 141–171. https://doi.org/10.1111/bre.12707

Pohl, F., Eggenhuisen, J.T., Cartigny, M.J.B., Tilston, M.C., de Leeuw, J., Hermidas, N., 2020a. The influence of a slope break on turbidite deposits: An experimental investigation. Marine Geology 424, 106160. https://doi.org/10.1016/j.margeo.2020.106160

Pohl, F., Eggenhuisen, J.T., Kane, I.A., Clare, M.A., 2020b. Transport and Burial of Microplastics in Deep-Marine Sediments by Turbidity Currents. Environ. Sci. Technol. 54, 4180–4189. https://doi.org/10.1021/acs.est.9b07527

Postma, G., Kleverlaan, K., 2018. Supercritical flows and their control on the architecture and facies of small-radius sand-rich fan lobes. Sedimentary Geology 364, 53–70. https://doi.org/10.1016/j.sedgeo.2017.11.015

Prather, B.E., 2020. Chapter 18 - Controls on reservoir distribution, architecture and stratigraphic trapping in slope settings, in: Scarselli, N., Adam, J., Chiarella, D., Roberts, D.G., Bally, A.W. (Eds.), Regional Geology and Tectonics (Second Edition). Elsevier, pp. 481–515. https://doi.org/10.1016/B978-0-444-64134-2.00025-0

Prather, B.E., Pirmez, C., Sylvester, Z., Prather, D.S., 2012. Stratigraphic Response to Evolving Geomorphology in a Submarine Apron Perched On the Upper Niger Delta Slope, in: Prather, B.E., Deptuck, M.E., Mohrig, D., Hoorn, B.V., Wynn, R.B. (Eds.), Application of the Principles of Seismic Geomorphology to Continental Slope and Base-of-Slope Systems: Case Studies from SeaFloor and Near-Sea Floor Analogues. SEPM Society for Sedimentary Geology, p. 0. https://doi.org/10.2110/pec.12.99.0145

Prélat, A., Covault, J.A., Hodgson, D.M., Fildani, A., Flint, S.S., 2010. Intrinsic controls on the range of volumes, morphologies, and dimensions of submarine lobes. Sedimentary Geology 232, 66–76. https://doi.org/10.1016/j.sedgeo.2010.09.010

Prélat, A., Hodgson, D.M., Flint, S.S., 2009. Evolution, architecture and hierarchy of distributary deep-water deposits: a high-resolution outcrop investigation from the Permian Karoo Basin, South Africa. Sedimentology 56, 2132–2154. https://doi.org/10.1111/j.1365-3091.2009.01073.x

Reading, H.G., Richards, M., 1994. Turbidite Systems in Deep-Water Basin Margins Classified by Grain Size and Feeder System 1. AAPG Bulletin 78, 792–822. https://doi.org/10.1306/A25FE3BF-171B-11D7-8645000102C1865D

Rohais, S., Bailleul, J., Brocheray, S., Schmitz, J., Paron, P., Kezirian, F., Barrier, P., 2021. Depositional Model for Turbidite Lobes in Complex Slope Settings Along Transform Margins: The Motta San Giovanni Formation (Miocene—Calabria, Italy). Frontiers in Earth Science 9.

Romans, B.W., Castelltort, S., Covault, J.A., Fildani, A., Walsh, J.P., 2016. Environmental signal propagation in sedimentary systems across timescales. Earth-Science Reviews, Source-to-Sink Systems: Sediment & Solute Transfer on the Earth Surface 153, 7–29. https://doi.org/10.1016/j.earscirev.2015.07.012

Saller, A., Werner, K., Sugiaman, F., Cebastiant, A., May, R., Glenn, D., Barker, C., 2008. Characteristics of Pleistocene deep-water fan lobes and their application to an upper Miocene reservoir model, offshore East Kalimantan, Indonesia. AAPG Bulletin 92, 919–949. https://doi.org/10.1306/03310807110

Schwab, W.C., Lee, H.J., Twichell, D.C., Locat, J., Nelson, C.H., McArthur, W.G., Kenyon, N.H., 1996. Sediment mass-flow processes on a depositional lobe, outer Mississippi Fan. Journal of Sedimentary Research 66, 916–927. https://doi.org/10.1306/D426843C-2B26-11D7-8648000102C1865D

Shi, C., Dong, C., Lin, C., Ren, L., Luan, G., Li, Y., 2021. A semi-confined turbidite system in the eocene lacustrine: An example from Niuzhuang Sag, Bohai Bay Basin, Eastern China. Journal of Petroleum Science and Engineering 206, 108924. https://doi.org/10.1016/j.petrol.2021.108924

Silva, T.A., Girardclos, S., Stutenbecker, L., Bakker, M., Costa, A., Schlunegger, F., Lane, S.N., Molnar, P., Loizeau, J.-L., 2019. The sediment budget and dynamics of a delta-canyon-lobe system over the Anthropocene timescale: The Rhone River delta, Lake Geneva (Switzerland/France). Sedimentology 66, 838–858. https://doi.org/10.1111/sed.12519

Sømme, T.O., Helland-Hansen, W., Martinsen, O.J., Thurmond, J.B., 2009. Relationships between morphological and sedimentological parameters in source-to-sink systems: a basis for predicting semi-quantitative characteristics in subsurface systems. Basin Research 21, 361–387. https://doi.org/10.1111/j.1365-2117.2009.00397.x

Spychala, Y.T., Poyatos-Moré, M., Blumenberg, M., Scheeder, G., Winsemann, J., 2025. Enrichment of organic carbon in a deep-water sand-prone turbidite system: A study from the Eocene Aínsa Basin (Spanish Pyrenees). Sedimentology 22. https://doi.org/10.1111/sed.70041

Straub, K.M., Pyles, D.R., 2012. Quantifying the Hierarchical Organization of Compensation In Submarine Fans Using Surface Statistics. Journal of Sedimentary Research 82, 889–898. https://doi.org/10.2110/jsr.2012.73

Sweet, M.L., Gaillot, G.T., Jouet, G., Rittenour, T.M., Toucanne, S., Marsset, T., Blum, M.D., 2019. Sediment routing from shelf to basin floor in the Quaternary Golo System of Eastern Corsica, France, western Mediterranean Sea. GSA Bulletin 132, 1217–1234. https://doi.org/10.1130/B35181.1

Syvitski, J.P.M., Milliman, J.D., 2007. Geology, Geography, and Humans Battle for Dominance over the Delivery of Fluvial Sediment to the Coastal Ocean. The Journal of Geology 115, 1–19. https://doi.org/10.1086/509246

Talling, P.J., 2014. On the triggers, resulting flow types and frequencies of subaqueous sediment density flows in different settings. Marine Geology, 50th Anniversary Special Issue 352, 155–182. https://doi.org/10.1016/j.margeo.2014.02.006

Talling, P.J., Baker, M.L., Pope, E.L., 2022. Longest sediment flows yet measured show how major rivers connect efficiently to deep sea. Nature communications, 2022, vol. 13, no 1, p. 4193. Nature Communications 13, 4193. https://doi.org/10.1038/s41467-022-31689-3

Talling, P.J., Hage, S., Baker, M.L., Bianchi, T.S., Hilton, R.G., Maier, K.L., 2024. The Global Turbidity Current Pump and Its Implications for Organic Carbon Cycling. Annual Review of Marine Science 16, 105–133. https://doi.org/10.1146/annurev-marine-032223-103626

Talling, P.J., Masson, D.G., Sumner, E.J., Malgesini, G., 2012. Subaqueous sediment density flows: Depositional processes and deposit types. Sedimentology 59, 1937–2003. https://doi.org/10.1111/j.1365-3091.2012.01353.x

Talling, P.J., Wynn, R.B., Schmmidt, D.N., Rixon, R., Sumner, E., Amy, L., 2010. How Did Thin Submarine Debris Flows Carry Boulder-Sized Intraclasts for Remarkable Distances Across Low Gradients to the Far Reaches of the Mississippi Fan? Journal of Sedimentary Research 80, 829–851. https://doi.org/10.2110/jsr.2010.076

Twichell, D., Nelson, C.H., Kenyon, N., Schwab, W., 2009. The Influence of External Processes on the Holocene Evolution of the Mississippi Fan, in: Kneller, B., Martinsen, O.J., McCaffrey, B. (Eds.), External Controls on Deep-Water Depositional Systems. SEPM Society for Sedimentary Geology, p. 0. https://doi.org/10.2110/sepmsp.092.145

Wahab, A., Hoyal, D.C., Shringarpure, M., Straub, K.M., 2022. A dimensionless framework for predicting submarine fan morphology. Nat Commun 13, 7563. https://doi.org/10.1038/s41467-022-34455-7

Wynn, R.B., Kenyon, N.H., Masson, D.G., Stow, D.A.V., Weaver, P.P.E., 2002. Characterization and Recognition of Deep-Water Channel-Lobe Transition Zones. AAPG Bulletin 86, 1441–1462. https://doi.org/10.1306/61EEDCC4-173E-11D7-8645000102C1865D

Zaragosi, S., Auffret, G.A., Voisset, M., Garlan, T., 2003. Morphology and Depositional Processes of the Celtic Fan, Bay of Biscay, in: Mienert, J., Weaver, P. (Eds.), European Margin Sediment Dynamics: Side-Scan Sonar and Seismic Images. Springer, Berlin, Heidelberg, pp. 239–243. https://doi.org/10.1007/978-3-642-55846-7_39

Zhang, J.-J., Wu, S.-H., Fan, T.-E., Fan, H.-J., Jiang, L., Chen, C., Wu, Q.-Y., Lin, P., 2016. Research on the architecture of submarine-fan lobes in the Niger Delta Basin, offshore West Africa. Journal of Palaeogeography 5, 185–204. https://doi.org/10.1016/j.jop.2016.05.005

Supplementary Materials 1. Table of the properties of the compared systems in this study.

System	Margin/basin type	Location (see also Fig. 2)	Age	Fan type	Ponding	System size if marine / else lacustrine	System size this work	Hierarchy	References
Al Batha	Passive	Oman Basin, Arabian Sea	Quaternary	Basin floor	Not ponded	Small	Small	H3, H4	Bourget et al. 2010
Alboran Sea Almeria	Active	Mediterranean Sea, offshore Spain	Late Pliocene/Quaternary	Basin floor	Not ponded	Small	Small	H4	Garcia et al., 2015; Alonso and Ercilla, 2002
Alboran Sea Sacratif	Active	Mediterranean Sea, offshore Spain	Late Pliocene/Quaternary	Basin floor	Not ponded	Small	Small	H4	Garcia et al., 2015; Alonso and Ercilla, 2002
Alboran Sea Salobrena	Active	Mediterranean Sea, offshore Spain	Late Pliocene/Quaternary	Basin floor	Not ponded	Small	Small	H4	Garcia et al., 2015
Alboran Sea Guadiaro	Active	Mediterranean Sea, offshore Spain	Late Pliocene/Quaternary	Basin floor	Not ponded	Small	Small	H4	Garcia et al., 2015; Alonso and Ercilla, 2002
Alboran Sea La Linea	Active	Mediterranean Sea, offshore Spain	Late Pliocene/Quaternary	Basin floor	Not ponded	Small	Small	H4	Garcia et al., 2015
Alboran Sea Calahonda	Active	Mediterranean Sea, offshore Spain	Late Pliocene/Quaternary	Basin floor	Not ponded	Small	Small	H4	Garcia et al., 2015
Alboran Sea Fuengirola	Active	Mediterranean Sea, offshore Spain	Late Pliocene/Quaternary	Basin floor	Not ponded	Small	Small	H4	Garcia et al., 2015
Alboran Sea Torrenueva	Active	Mediterranean Sea, offshore Spain	Late Pliocene/Quaternary	Basin floor	Not ponded	Small	Small	H4	Garcia et al., 2015
Alboran Sea Banos	Active	Mediterranean Sea, offshore Spain	Late Pliocene/Quaternary	Basin floor	Not ponded	Small	Small	H4	Garcia et al., 2015
Anotz Fm	Active	Pamplune Basin, onshore Spain	Eocene	Basin floor	Not ponded	Small (coarse-grained)	Small	H4	Payros et al. 2007
Bering Turbidite System	Passive	Bering Sea, Offshore Alaska, USA	Unknown	Basin floor	Not ponded	Intermediate	Large	H4	Kenyon and Millington, 1995
Unmak Turbidite System	Passive	Bering Sea, Offshore Alaska, USA	Unknown	Basin floor	Not ponded	Intermediate	Large	H4	Kenyon and Millington, 1995
Pichnol Turbidite System	Passive	Bering Sea, Offshore Alaska, USA	Unknown	Basin floor	Not ponded	Intermediate	Large	H4	Kenyon and Millington, 1995
Bering Sea B1	Passive	Bering Sea, Offshore Alaska, USA	Unknown	Basin floor	Not ponded	Intermediate	Large	H4	Kenyon and Millington, 1995
Bering Sea B2	Passive	Bering Sea, Offshore Alaska, USA	Unknown	Basin floor	Not ponded	Intermediate	Large	H4	Kenyon and Millington, 1995
Bering Sea B3	Passive	Bering Sea, Offshore Alaska, USA	Unknown	Basin floor	Not ponded	Intermediate	Large	H4	Kenyon and Millington, 1995
Bering Sea B4	Passive	Bering Sea, Offshore Alaska, USA	Unknown	Basin floor	Not ponded	Intermediate	Large	H4	Kenyon and Millington, 1995
Brazos-Trinity Basin II and IV	Passive	Offshore Texas, USA	Late Pleistocene	Intraslope	Ponded	Small	Small	H3, H4	Beaubouef and Friedman 2000; Beaubouef et al. 2003a; 2003b
Bute Inlet	Passive	British Columbia, Canada (fjord)	Quaternary	Intraslope	Not ponded	Small	Small	H3	Prior et al., 1986; 1987; Syvitski and Farrow, 1983
Campos Basin "lobo"	Passive	Southern Atlantic, Offshore Brazil	Holocene	Basin floor	Not ponded	Small	Small	H4	Machado et al. 2004
Campos Basin Albacora	Passive	Southern Atlantic, Offshore Brazil	Oligo-Miocene	Intraslope	Ponded	Small	Small	H4	Casagrande 2023
Campos Basin Barracuda	Passive	Southern Atlantic, Offshore Brazil	Oligo-Miocene	Intraslope	Ponded	Small	Small	H3, H4	Assis et al. 1998
Campos Basin Marlim Sul	Passive	Southern Atlantic, Offshore Brazil	Oligo-Miocene	Intraslope	Ponded	Small	Small	H4	Casagrande et al. 2024
Campos Basin Marlim	Passive	Southern Atlantic, Offshore Brazil	Oligo-Miocene	Intraslope	Ponded	Small	Small	H3	Casagrande et al. 2022
Campos Basin unknown	Passive	Southern Atlantic, Offshore Brazil	Oligo-Miocene	Intraslope	Ponded	Small	Small	H3	Bruhn et al. 1998
Catalina Basin	Transform	Offshore California, USA	Quaternary	Intraslope	Not ponded	Small	Small	H2	Maier et al. 2018
Celtic fan	Passive	Bay of Biscay, Offshore Ireland	Quaternary	Basin floor	Not ponded	Intermediate	Large	H3, H4	Zaragosi et al. 2003
Congo Axial Fan	Passive	Southern Atlantic, Offshore Congo/Angola	Late Quaternary	Basin floor	Not ponded	Large	Large	H3, H4	Babonneau 2002; Picot et al. 2016; Dennielou et al. 2017
East Corsica South Golo	Active	Offshore East Corsica, France	Late Pleistocene	Basin floor	Not ponded	Small	Small	H2, H3, H4	Deptuck et al. 2008; Sweet et al. 2019
East Corsica North Golo	Active	Offshore East Corsica, France	Late Pleistocene	Basin floor	Not ponded	Small	Small	H2, H3, H4	Deptuck et al. 2008; Sweet et al. 2019
East Corsica Fiuminale	Active	Offshore East Corsica, France	Late Pleistocene	Basin floor	Not ponded	Small	Small	H4	Deptuck et al. 2008; Sweet et al. 2019
East Corsica St Damiano	Active	Offshore East Corsica, France	Late Pleistocene	Basin floor	Not ponded	Small	Small	H4	Sweet et al. 2019
East Corsica Pineto	Active	Offshore East Corsica, France	Late Pleistocene	Intraslope	Not ponded	Small	Small	H3	Deptuck et al. 2008
Geneva Lake	Post-glacial lake	Onshore France and Switzerland	Late Quaternary	Basin floor	Not ponded	Lacustrine	Lacustrine	H3lac	Silva et al. 2019
Gendalo	Passive	Offshore Borneo, Indonesia	Upper Miocene	Basin floor	Not ponded	Small	Small	H2, H3	Saller et al. 2008
Gulf of Cadiz Aveiro	Active	Offshore Spain	Late Quaternary	Intraslope	Not ponded	Small	Small	H2, H3	Hanquiez et al. 2010
Gulf of Cadiz Lolita	Active	Offshore Spain	Late Quaternary	Intraslope	Not ponded	Small	Small	H2, H3	Hanquiez et al. 2010
Gulf of Cadiz Tasyo	Active	Offshore Spain	Late Quaternary	Intraslope	Not ponded	Small	Small	H2, H3	Hanquiez et al. 2010
Karoo Tanqua Fan 3	Passive	Onshore South Africa	Permian	Basin floor	Not ponded	Small	Small	H2, H3, H4	Prelat et al. 2009; 2010
Karoo Lainsburg	Passive	Onshore South Africa	Permian	Both	Not ponded	Small	Small	H3	Brooks et al. 2018
Kutai Basin	Passive	Offshore Borneo, Indonesia	Pleistocene	Basin floor	Not ponded	Small	Small	H2, H3, H4	Saller et al. 2008
Falkland Basin	Aborted	Faroe-Shetland Trough, Northern Atlantic	Early Cretaceous	Basin floor	Not ponded	Lacustrine	Lacustrine	H3lac, H4lac	Dodd et al. 2019
La Fonta	Passive	Mediterranean Sea, Offshore France	Holocene	Basin floor	Not ponded	Small	Small	H4	Droz et al., 2001; 2006
Reserve Fan	Post-glacial lake	Lake Superior, Minessota, USA	Holocene	Basin floor	Not ponded	Lacustrine	Lacustrine	H3lac	Normark and Dickson 1976a; 1976b
Mississippi	Passive	Offshore Louisiana, USA	Plio-Pleistocene	Basin floor	Not ponded	Large	Large	H2, H4	Stelting et al. 1986; Twichell et al. 1991; 2009; Wen et al. 1995
Myanmar	Active	Offshore Myanmar (Bay of Bengal)	Pliocene	Basin floor	Not ponded	Small	Small	H3, H4	Yang and Kim 2014, Cossey et al. 2013
Molasse Basin	Active	Onshore Austria	Miocene	Intraslope	Ponded	Small (coarse-grained)	Small	H4	De Ruig and Hubbard 2006
Monterey fan	Transform	Offshore California, USA	Late Pliocene	Basin floor	Not ponded	Intermediate	Large	H3	Wilde et al 1978; Fildani and Normark, 2004
Navy fan	Transform	Offshore California, USA	Late Pliocene-Holocene	Basin floor	Not ponded	Small	Small	H3	Piper and Normark. 1983
New Zealand	Active	Onshore New Zealand	Miocene	Intraslope	Not ponded	Small	Small	H4	Burgreen and Graham 2014
New Zealand	Active	Offshore New Zealand	Miocene	Intraslope	Ponded	Small	Small	H4	McArthur et al. 2021
Nigeria "basin floor LC"	Passive	Southern Atlantic, Offshore Nigeria	Miocene	Basin floor	Not ponded	Large	Small	H3, H4	Zhang et al. 2016
Nigeria OML 140	Passive	Southern Atlantic, Offshore Nigeria	Quaternary	Basin floor	Not ponded	Large	Small	H3, H4	Prélat et al. 2010
Nigeria X Fan	Passive	Southern Atlantic, Offshore Nigeria	Quaternary	Intraslope	Ponded	Large	Small	H2, H3, H4	Prather et al., 2012; Jobe et al. 2017
Nigeria intraslope LC	Passive	Southern Atlantic, Offshore Nigeria	Miocene	Intraslope	Ponded	Large	Small	H3, H4	Zhang et al., 2016
Nigeria intraslope LC	Passive	Southern Atlantic, Offshore Nigeria	Late Miocene	Intraslope	Ponded	Large	Small	H4	Pizzi, 2019; Pizzi et al. 2023
Nigeria intraslope lobes	Passive	Southern Atlantic, Offshore Nigeria	Late Miocene	Intraslope	Ponded	Large	Small	H3	Pizzi et al. 2023
Nile	Passive	Mediterranean Sea, Offshore Egypt	Quaternary	Basin floor	Not ponded	Large	Large	H4	Migeon et al. 2010
Nile intraslope	Passive	Mediterranean Sea, Offshore Egypt	Pliocene	Intraslope	Not ponded	Small	Small	H3	Li et al., 2021
Rhone fan and Neofan	Passive	Mediterranean Sea, Offshore France	Plio-Pleistocene	Basin floor	Not ponded	Intermediate	Large	H3	Jegou, 2008; Droz et al. 2020
South Korea	Active	Onshore South Korea	Miocene	Basin floor	Not ponded	Small	Small	H3	Kim and Chough 2000
Niugzhang Sag	Aborted	Onshore Eastern China	Eocene	Basin floor	Not ponded	Lacustrine	Lacustrine	H3lac	Shi et al., 2021
Western Shetland	Inverted	Faroe-Shetland Trough, Northern Atlantic	Early Eocene	Basin floor	Not ponded	Small	Small	H4	Kjøller 2015

References cited in Table SM1.

Alonso, B., Ercilla, G., 2002. Small turbidite systems in a complex tectonic setting (SW Mediterranean Sea): morphology and growth patterns. Marine and Petroleum Geology 19, 1225–1240. https://doi.org/10.1016/S0264-8172(03)00036-9

Assis, O.C., Becker, M.R., Melo, J.R.C., Franz, E.P., Alves, R.R.P., Rodriguez, M.R., Maciel, W.B., Souza, O.G.Jr., Johann, P.R.S., 1998. Barracuda and Caratinga giant oil fields, deep water Campos Basin, Brazil, in: Offshore Technology Conference. Presented at the Offshore Technology Conference, Houston, Texas, p. 7.

Babonneau, N., 2002. Mode de fonctionnement d'un chenal turbiditique méandriforme: Cas du Système Turbiditique Actuel du Zaïre. Université de Bordeaux I, p. 308.

Beaubouef, R.T., Abreu, V.S., Van Wagoner, J.C., 2003a. Basin 4 of the Brazos-trinity Slope System, Western Gulf of Mexico: The Terminal Portion of a Late Pleistocene Lowstand System Tract, in: Shelf Margin Deltas and Linked Down Slope Petroleum Systems: Global Significance and Future Exploration Potential. pp. 48–69.

Beaubouef, R.T., Friedmann, S.J., 2000. High Resolution Seismic/Sequence Stratigraphic Framework for the Evolution of Pleistocene Intra Slope Basins, Western Gulf of Mexico: Depositional Models and Reservoir Analogs, in: Weimer, P. (Ed.), Deep-Water Reservoirs of the World. SEPM Society for Sedimentary Geology, p. 0. https://doi.org/10.5724/gcs.00.15.0040

Beaubouef, R.T., Van Wagoner, J.C., Adair, N.L., 2003b. Ultra-High Resolution 3-D Characterization of Deep-Water Deposits- II: Insights into the Evolution of a Submarine Fan and Comparisons with River Deltas*. Search and Discovery Article 8.

Bourget, J., Zaragosi, S., Mulder, T., Schneider, J.-L., Garlan, T., Van Toer, A., Mas, V., Ellouz-Zimmermann, N., 2010. Hyperpycnal-fed turbidite lobe architecture and recent sedimentary processes: A case study from the Al Batha turbidite system, Oman margin. Sedimentary Geology 229, 144–159. https://doi.org/10.1016/j.sedgeo.2009.03.009

Brooks, H.L., Hodgson, D.M., Brunt, R.L., Peakall, J., Poyatos-Moré, M., Flint, S.S., 2018. Disconnected submarine lobes as a record of stepped slope evolution over multiple sea-level cycles. Geosphere 14, 1753–1779. https://doi.org/10.1130/GES01618.1

Bruhn, C.H.L., Arienti, L.M., Castro, D.D., Adams, T., Barros, A.P., Sarzenski, D.J., Camoleze, Z., 1998. Reservoir characterization of Oligocene/Miocene sand-rich turbidites from deep-water Campos Basin, Brazil. Presented at the AAPG International Conference & Exhibition, AAPG, Rio de Janeiro, Brazil, p. 30.

Burgreen, B., Graham, S., 2014. Evolution of a deep-water lobe system in the Neogene trench-slope setting of the East Coast Basin, New Zealand: Lobe stratigraphy and architecture in a weakly confined basin configuration. Marine and Petroleum Geology 54, 1–22. https://doi.org/10.1016/j.marpetgeo.2014.02.011

Casagrande, J., 2023. Evolution of submarine channel and lobe systems above dynamic stepped slopes. The University of Leeds.

Casagrande, J., Hodgson, D.M., Peakall, J., 2024. A salty snapshot: extreme variations in basal erosion patterns preserved in a submarine channel. Journal of the Geological Society 181, jgs2023-006. https://doi.org/10.1144/jgs2023-006

Casagrande, J., Hodgson, D.M., Peakall, J., Benac, P.M., 2022. Fill-and-Spill, Tilt-and-Repeat (FaSTaR) cycles: Stratigraphic evolution above a dynamic submarine stepped slope. Basin Research 34, 2162–2188. https://doi.org/10.1111/bre.12700

Cossey, S., Kim, D., Yang, S.-Y., Jung, H.Y., 2013. The Identification and Implication of Injectites in the Shwe Gas Field, Offshore Northwestern Myanmar; #20225 (2013). Search and Discovery Article 20225, 25.

Dennielou, B., Droz, L., Babonneau, N., Jacq, C., Bonnel, C., Picot, M., Le Saout, M., Saout, Y., Bez, M., Savoye, B., Olu, K., Rabouille, C., 2017. Morphology, structure, composition and build-up processes of the active channel-mouth lobe complex of the Congo deep-sea fan with inputs from remotely operated underwater vehicle (ROV) multibeam and video surveys. Deep Sea Research Part II: Topical Studies in Oceanography, Organic carbon transfer and ecosystem functioning in

the terminal lobes of the Congo deep-sea fan: The Conglobe multidisciplinary study 142, 25–49. https://doi.org/10.1016/j.dsr2.2017.03.010

Deptuck, M.E., Piper, D.J.W., Savoye, B., Gervais, A., 2008. Dimensions and architecture of late Pleistocene submarine lobes off the northern margin of East Corsica. Sedimentology 55, 869–898. https://doi.org/10.1111/j.1365-3091.2007.00926.x

Dodd, T.J.H., McCarthy, D.J., Richards, P.C., 2019. A depositional model for deep-lacustrine, partially confined, turbidite fans: Early Cretaceous, North Falkland Basin. Sedimentology 66, 53–80. https://doi.org/10.1111/sed.12483

Droz, L., dos Reis, A.T., Rabineau, M., Berné, S., Bellaiche, G., 2006. Quaternary turbidite systems on the northern margins of the Balearic Basin (Western Mediterranean): a synthesis. Geo-Mar Lett 26, 347–359. https://doi.org/10.1007/s00367-006-0044-0

Droz, L., Jégou, I., Gillet, H., Dennielou, B., Bez, M., Canals, M., Amblas, D., Lastras, G., Rabineau, M., 2020. On the termination of deep-sea fan channels: Examples from the Rhône Fan (Gulf of Lion, Western Mediterranean Sea). Geomorphology 369, 107368. https://doi.org/10.1016/j.geomorph.2020.107368

Droz, L., Kergoat, R., Cochonat, P., Berné, S., 2001. Recent sedimentary events in the western Gulf of Lions (Western Mediterranean). Marine Geology 176, 23–37. https://doi.org/10.1016/S0025-3227(01)00147-5

Fildani, A., Normark, W.R., 2004. Late Quaternary evolution of channel and lobe complexes of Monterey Fan. Marine Geology 206, 199–223. https://doi.org/10.1016/j.margeo.2004.03.001

Garcia, M., Ercilla, G., Alonso, B., Estrada, F., Jane, G., Mena, A., Alves, T., Juan, C., 2015. Deep-water turbidite systems: a review of their elements, sedimentary processes and depositional models. Their characteristics on the Iberian margins - Sistemas turbidíticos de aguas profundas: revisión de sus elementos, procesos sedimentarios y modelos deposicionales. Sus características en los márgenes Ibéricos. Boletín Geológico y Minero 126, 189–218.

Hanquiez, V., Mulder, T., Toucanne, S., Lecroart, P., Bonnel, C., Marchès, E., Gonthier, E., 2010. The sandy channel–lobe depositional systems in the Gulf of Cadiz: Gravity processes forced by contour current processes. Sedimentary Geology, Lobes in deep-sea turbidite systems 229, 110–123. https://doi.org/10.1016/j.sedgeo.2009.05.008

Jegou, I., 2008. Etude de la transition chenal-levées/lobe dans les systèmes turbiditiques récents. Application à l'éventail turbiditique de l'Amazone et au Néofan du Petit-Rhône. Université de Brest.

Jobe, Z.R., Sylvester, Z., Howes, N., Pirmez, C., Parker, A., Cantelli, A., Smith, R., Wolinsky, M.A., O'Byrne, C., Slowey, N., Prather, B., 2017. High-resolution, millennial-scale patterns of bed compensation on a sand-rich intraslope submarine fan, western Niger Delta slope. GSA Bulletin 129, 23–37. https://doi.org/10.1130/B31440.1

Kenyon, N.H., Millington, J., 1995. Contrasting deep-sea depositional systems in the Bering Sea, in: Pickering, K.T., Hiscott, R.N., Kenyon, N.H., Ricci Lucchi, F., Smith, R.D.A. (Eds.), Atlas of Deep Water Environments: Architectural Style in Turbidite Systems. Springer Netherlands, Dordrecht, pp. 196–202. https://doi.org/10.1007/978-94-011-1234-5_28

Kim, J.W., Chough, S.K., 2000. A gravel lobe deposit in the prodelta of the Doumsan fan delta (Miocene), SE Korea. Sedimentary Geology 130, 183–203. https://doi.org/10.1016/S0037-0738(99)00111-6

Kjøller, H.E., 2015. Source-to-sink system analysis of a modern submarine sedimentary system, Judd/FLett Sub-basins, west of Shetland. A possible analogue to ancient Paleocene subsurface sedimentary systems. (M.S. thesis). University of Copenhagen.

Li, P., Kneller, B., Hansen, L., 2021. Anatomy of a gas-bearing submarine channel-lobe system on a topographically complex slope (offshore Nile Delta, Egypt). Marine Geology 437, 106496. https://doi.org/10.1016/j.margeo.2021.106496

Machado, L.C.R., Kowsmann, R.O., Almeida, W.Jr., Murakami, C.Y., Schreiner, S., Miller, D.J., Piaiolino, P.O.V., 2004. Geometria da porçao proximal do sistema deposicional turbiditico moderno da Formaçao Carapebus, Bacia de Campos; modelo para heterogeneidades de reservatorio Geometry. Boletim de Geociências da Petrobras 12, 287–315.

Maier, K.L., Johnson, S.Y., Hart, P., 2018. Controls on submarine canyon head evolution: Monterey Canyon, offshore central California. Marine Geology 404, 24–40. https://doi.org/10.1016/j.margeo.2018.06.014

McArthur, A.D., Bailleul, J., Mahieux, G., Claussmann, B., Wunderlich, A., McCaffrey, W.D., 2021. Deformation–sedimentation feedback and the development of anomalously thick aggradational turbidite lobes: Outcrop and subsurface examples from the Hikurangi Margin, New Zealand. Journal of Sedimentary Research 91, 362–389. https://doi.org/10.2110/jsr.2020.013

Migeon, S., Ducassou, E., Le Gonidec, Y., Rouillard, P., Mascle, J., Revel-Rolland, M., 2010. Lobe construction and sand/mud segregation by turbidity currents and debris flows on the western Nile deep-sea fan (Eastern Mediterranean). Sedimentary Geology, Lobes in deep-sea turbidite systems 229, 124–143. https://doi.org/10.1016/j.sedgeo.2010.02.011

Normark, W.R., Dickson, F.H., 1976a. Man-made turbidity currents in Lake Superior. Sedimentology 23, 815–831. https://doi.org/10.1111/j.1365-3091.1976.tb00110.x

Normark, W.R., Dickson, F.H., 1976b. Sublacustrine Fan Morphology in Lake Superior1. AAPG Bulletin 60, 1021–1036. https://doi.org/10.1306/C1EA360E-16C9-11D7-8645000102C1865D

Payros, A., Pujalte, V., Orue-Etxebarria, X., 2007. A point-sourced calciclastic submarine fan complex (Eocene Anotz Formation, western Pyrenees): facies architecture, evolution and controlling factors. Sedimentology 54, 137–168. https://doi.org/10.1111/j.1365-3091.2006.00823.x

Picot, M., Droz, L., Marsset, T., Dennielou, B., Bez, M., 2016. Controls on turbidite sedimentation: Insights from a quantitative approach of submarine channel and lobe architecture (Late Quaternary Congo Fan). Marine and Petroleum Geology 72, 423–446. https://doi.org/10.1016/j.marpetgeo.2016.02.004

Piper, D.J.W., Normark, W.R., 1983. Turbidite depositional patterns and flow characteristics, Navy Submarine Fan, California Borderland. Sedimentology 30, 681–694. https://doi.org/10.1111/j.1365-3091.1983.tb00702.x

Pizzi, M., 2019. Quantification of tectonic controls on the distribution and architecture of deep-water facies during the growth of the toe-thrusts region of the Niger Delta. https://doi.org/10.25560/85679

Pizzi, M., Whittaker, A.C., Mayall, M., Lonergan, L., 2023. Structural controls on the pathways and sedimentary architecture of submarine channels: New constraints from the Niger Delta. Basin Research 35, 141–171. https://doi.org/10.1111/bre.12707

Prather, B.E., Pirmez, C., Sylvester, Z., Prather, D.S., 2012. Stratigraphic Response to Evolving Geomorphology in a Submarine Apron Perched On the Upper Niger Delta Slope, in: Prather, B.E., Deptuck, M.E., Mohrig, D., Hoorn, B.V., Wynn, R.B. (Eds.), Application of the Principles of Seismic Geomorphology to Continental Slope and Base-of-Slope Systems: Case Studies from SeaFloor and Near-Sea Floor Analogues. SEPM Society for Sedimentary Geology, p. 0. https://doi.org/10.2110/pec.12.99.0145

Prélat, A., Covault, J.A., Hodgson, D.M., Fildani, A., Flint, S.S., 2010. Intrinsic controls on the range of volumes, morphologies, and dimensions of submarine lobes. Sedimentary Geology 232, 66–76. https://doi.org/10.1016/j.sedgeo.2010.09.010

Prélat, A., Hodgson, D.M., Flint, S.S., 2009. Evolution, architecture and hierarchy of distributary deep-water deposits: a high-resolution outcrop investigation from the Permian Karoo Basin, South Africa. Sedimentology 56, 2132–2154. https://doi.org/10.1111/j.1365-3091.2009.01073.x

Prior, D.B., Bornhold, B.D., Johns, M.W., 1986. Active sand transport along a fjord-bottom channel, Bute Inlet, British Columbia. Geology 14, 581–584. https://doi.org/10.1130/0091-7613(1986)14%253C581:ASTAAF%253E2.0.CO;2

Prior, D.B., Bornhold, B.D., Wiseman, W.J., Lowe, D.R., 1987. Turbidity Current Activity in a British Columbia Fjord. Science 237, 1330–1333. https://doi.org/10.1126/science.237.4820.1330

Ruig, M.J.D., Hubbard, S.M., 2006. Seismic facies and reservoir characteristics of a deep-marine channel belt in the Molasse foreland basin, Puchkirchen Formation, Austria. AAPG Bulletin 90, 735–752. https://doi.org/10.1306/10210505018

Saller, A., Werner, K., Sugiaman, F., Cebastiant, A., May, R., Glenn, D., Barker, C., 2008. Characteristics of Pleistocene deep-water fan lobes and their application to an upper Miocene reservoir model, offshore East Kalimantan, Indonesia. AAPG Bulletin 92, 919–949. https://doi.org/10.1306/03310807110

Shi, C., Dong, C., Lin, C., Ren, L., Luan, G., Li, Y., 2021. A semi-confined turbidite system in the eocene lacustrine: An example from Niuzhuang Sag, Bohai Bay Basin, Eastern China. Journal of Petroleum Science and Engineering 206, 108924. https://doi.org/10.1016/j.petrol.2021.108924

Silva, T.A., Girardclos, S., Stutenbecker, L., Bakker, M., Costa, A., Schlunegger, F., Lane, S.N., Molnar, P., Loizeau, J.-L., 2019. The sediment budget and dynamics of a delta-canyon-lobe system over the Anthropocene timescale: The Rhone River delta, Lake Geneva (Switzerland/France). Sedimentology 66, 838–858. https://doi.org/10.1111/sed.12519

Stelting, C.E., Droz, L., Bouma, A.H., Coleman, J.M., Cremer, M., Meyer, A.W., Normark, W.R., O'Connell, S., Stow, D.A.V., 1986. Late Pleistocene seismic stratigraphy of the Mississippi Fan, in: Initial Reports of the Deep Sea Drilling Project, 96. pp. 437–456.

Sweet, M.L., Gaillot, G.T., Jouet, G., Rittenour, T.M., Toucanne, S., Marsset, T., Blum, M.D., 2019. Sediment routing from shelf to basin floor in the Quaternary Golo System of Eastern Corsica, France, western Mediterranean Sea. GSA Bulletin 132, 1217–1234. https://doi.org/10.1130/B35181.1

Syvitski, J.P.M., Farrow, G.E., 1983. Structures and processes in bayhead deltas: Knight and bute inlet, British Columbia. Sedimentary Geology 36, 217–244. https://doi.org/10.1016/0037-0738(83)90010-6

Twichell, D., Nelson, C.H., Kenyon, N., Schwab, W., 2009. The Influence of External Processes on the Holocene Evolution of the Mississippi Fan, in: Kneller, B., Martinsen, O.J., McCaffrey, B. (Eds.), External Controls on Deep-Water Depositional Systems. SEPM Society for Sedimentary Geology, p. 0. https://doi.org/10.2110/sepmsp.092.145

Twichell, D.C., Kenyon, N.H., Parson, L.M., McGregor, B.A., 1991. Depositional Patterns of the Mississippi Fan Surface: Evidence from GLORIA II and High-Resolution Seismic Profiles, in: Weimer, P., Link, M.H. (Eds.), Seismic Facies and Sedimentary Processes of Submarine Fans and Turbidite Systems. Springer, New York, NY, pp. 349–363. https://doi.org/10.1007/978-1-4684-8276-8_19

Wen, R., Sinding-Larsen, R., Kenyon, N.H., 1995. Computer enhanced GLORIA sidescan sonar images of the surface of the Mississippi Fan, in: Pickering, K.T., Hiscott, R.N., Kenyon, N.H., Ricci Lucchi, F., Smith, R.D.A. (Eds.), Atlas of Deep Water Environments: Architectural Style in Turbidite Systems. Springer Netherlands, Dordrecht, pp. 297–299. https://doi.org/10.1007/978-94-011-1234-5_44

Wilde, P., Normark, W. R., Chase, T.E., 1978. Channel Sands and Petroleum Potential of Monterey Deep-Sea Fan, California. AAPG Bulletin 62, 967–983. https://doi.org/10.1306/C1EA4F7C-16C9-11D7-8645000102C1865D

Yang, S.-Y., Kim, J.W., 2014. Pliocene basin-floor fan sedimentation in the Bay of Bengal (offshore northwest Myanmar). Marine and Petroleum Geology 49, 45–58. https://doi.org/10.1016/j.marpetgeo.2013.09.007

Zaragosi, S., Auffret, G.A., Voisset, M., Garlan, T., 2003. Morphology and Depositional Processes of the Celtic Fan, Bay of Biscay, in: Mienert, J., Weaver, P. (Eds.), European Margin Sediment Dynamics: Side-Scan Sonar and Seismic Images. Springer, Berlin, Heidelberg, pp. 239–243. https://doi.org/10.1007/978-3-642-55846-7_39

Zhang, J.-J., Wu, S.-H., Fan, T.-E., Fan, H.-J., Jiang, L., Chen, C., Wu, Q.-Y., Lin, P., 2016. Research on the architecture of submarine-fan lobes in the Niger Delta Basin, offshore West Africa. Journal of Palaeogeography 5, 185–204. https://doi.org/10.1016/j.jop.2016.05.005